



Acid Activation of Natural Reed Filter Biomass (*Typha latifolia*) Application to Pb (II) Uptake from Aqueous Solutions: Kinetic, Thermodynamic Equilibrium Studies and Optimization Studies

Abdelhay El Amri¹ · Rachid Hsisou² · Assia Jebli¹ · Iman Lebki¹ · Jaouad Bensalah¹ · Fatima Zahra Bouhassane¹ · Lamiae Alami¹ · Azeddine Lebki¹ · Abdelkader Zarrouk³ · El Housseine Rifi¹ · Ahmed Lebki¹

Received: 11 March 2023 / Accepted: 28 June 2023 / Published online: 19 July 2023
© The Tunisian Chemical Society and Springer Nature Switzerland AG 2023

Abstract

This research looks at the potential use of natural biomass of fibers plant with raw leaf release (*Tl*) and sulphuric acid treated fibers (*Tls*) as adsorbents for the removal of Pb (II) ions in water. The properties of the materials were evaluated using X-ray diffraction (XRD), scanning electron microscopy (SEM), Fourier transform infrared spectrometry (FTIR), nitrogen adsorption–desorption isotherms and thermogravimetric analysis/differential thermogravimetry (TGA/DTG). investigations were used to describe the fundamental physicochemical characteristics of *Tl* both before and after acid treatment. Was the subject of bath adsorption tests Pb (II). The initial concentration of Pb (II) ions, reaction time, adsorbent dosage, and pH of the ions were all optimized. The calculated adsorption capacities of *Tl* and *Tls* on Pb (II) were 32.64 and 44.65 mg g⁻¹, respectively, according to adsorption isotherm studies. Under ideal biosorption circumstances, which include pH = 5, a biosorbent mass of 0.1 g, and an initial Pb²⁺ ion concentration of 10 ppm, calculations using the response surface methodology revealed a maximum biosorption efficiency of Pb²⁺ of 77.6% for *Tl* and 98.7% for *Tls*. Desorption research findings demonstrated the potential for promising regenerations, as the percentage removal of Pb (II) from the initial value was sustained at more than 60% even after three adsorption–desorption cycles. Furthermore, the adsorption expenses for Pb (II) removal using *Tl* and *Tls* were assumed to be 2.14 and 6.71 USD kg⁻¹, respectively. Based on these findings, *Tl* and *Tls* treated substances could be utilized as low-cost, environmentally friendly, and effective adsorbents for the removal of Pb (II) from water. G°, S°, and H° thermodynamic parameters demonstrated that the adsorption process was viable, spontaneous, and exothermic.

Keywords Low-cost adsorbents · BBD-RSM modeling · Pb (II) removal · Isotherms · Kinetics · Thermodynamics

1 Introduction

Due to their toxicity and harmful effects on both humans and other living things, lead, cadmium, mercury, and arsenic pose the greatest risks to human health when they are exposed to them in the environment. Because it may build up in both individual organisms and entire food chains, lead is a very toxic element [1]. Because of lead's high gastrointestinal absorption capacity and ability to cross the blood–brain barrier, children are especially vulnerable to exposure. Wastewater emissions from lead mining, metal plating, metal alloy manufacture, and acid battery production all contain lead. Several processes and technologies, such as ion exchange, evaporation and concentration, chemical precipitation, reverse osmosis, adsorption, and electro-dialysis, have been proposed to remove heavy metal ions from wastewater [2]. There are several physical, chemical

✉ Abdelhay El Amri
abdelhay.elamri@uit.ac.ma

✉ Rachid Hsisou
r.hsisou@gmail.com; hsisou.r@ucd.ac.ma

¹ Laboratory of Advanced Materials and Process Engineering (LAMPE), Department of Chemistry, Faculty of Sciences, Ibn Tofail University, B.P. 133, 14000 Kenitra, Morocco

² Laboratory of Organic Chemistry, Bioorganic and Environment, Chemistry Department, Faculty of Sciences, Chouaib Doukkali University, BP 20, 24000 El Jadida, Morocco

³ Laboratory of Materials, Nanotechnology and Environment, Faculty of Sciences, Mohammed V University in Rabat, Av. Ibn Battouta, P.O. Box. 1014, Agdal-Rabat, Morocco

and biological methods for treating and bleaching polluted effluents such as coagulation and flocculation, biodegradation, filtration membrane, chemical oxidation, ozonation, ion exchange, methods electrochemical and adsorption [3]. The adsorption technique is the most favorable method for the elimination of metallic trace elements has become an analytical method of choice, very effective and simple to use [4]. The principle of adsorption treatment is to trap the dyes by a solid material called adsorbent. In the literature, there are several solid materials (clays, zeolites, activated aluminas, sludge, biomass, agricultural residues, industrial by-products and coal active...) that can be used in water discoloration processes [5]. Research is focused on the use of low-cost adsorbents, available locally, biodegradable adsorbent, made from natural sources, these years, activated carbons synthesized from agricultural residues have been widely used as an adsorbent to treat colored effluents due to their porous structure very important, their large specific surface and their high adsorption capacity [6]. The recovery of agricultural residues, without generating pollutants is a great challenge and is recommended for sustainable industrial development to preserve the environment. All cheap materials such as biomass waste: apple peel, date pits [7], olive pits, peach pits [3] corn cobs, coffee beans and coffee grounds, tea waste, bagasse, coconut shell and apricot kernels [8] with a high content of carbon can be used as precursors for the production of activated carbon. These less expensive and renewable precursors compared to commercial activated carbon [9]. *Typha latifolia* fibers can be used as an adsorbent material to remove heavy metals, despite the fact that they have traditionally been considered in large quantities as forest waste [10]. Compared to unmodified *Typha latifolia* (Tl) biopolymer, modified or treated *Typha latifolia* (Tls) biopolymer compounds can increase the adsorption capacities of heavy metal ions.

2 Materials and Methods

2.1 Preparation of the Adsorbent

The investigated biomass of the Broad-leaved Massette (*Typha latifolia*), a reed filter plant, originated in Morocco and was collected in September 2020 from "Oued sabou" in Kenitra. To get rid of different pollutants like sand and grime, the reeds were cleansed using demineralized water. After that, the reeds were dried outside for 48 h. To obtain homogenous grains, the dried samples were sieved over a 250 μm size range. The sieved media was then placed in a sealed plastic container and kept there until it was time to treat it with 40% sulphuric acid at a 6:1 liquid to solid ratio. A magnetic stirrer was used to agitate the reaction mixture for 12 h at 60 °C. After that, demineralized water was used

to filter and repeatedly wash the acid-treated reeds. After being thoroughly cleaned, the reeds were dried for 24 h at 100 °C and utilized to establish their physical and chemical properties.

2.2 Chemical Products, Reagents and Analytical Methods

All of the compounds utilized in this research were reagent grade and were used without further purification (obtained from Sigma Aldrich). Lead nitrate and the corresponding distilled acids were dissolved in demineralized water to produce aqueous solutions of $\text{Pb}(\text{NO}_3)_2 \cdot 5 \text{H}_2\text{O}$ and HCl. A digital pH meter (Orion5Star) was employed to determine the pH levels. A spectrophotometer for atomic absorption (VARIAN AA240) was utilized to quantify the concentration of Pb^{2+} ions. Using a Hitachi 4700 SEM microscope, scanning electron micrographs were taken to examine the surface morphology of untreated and sulphuric acid-treated reed fibers. IR samples were obtained as pellets incorporating KBr using a Thermo Nicolet 8700 FT-IR spectrometer in the 4000–500 cm^{-1} band in transmission mode and under standard conditions.

2.3 Adsorption Experiments

Batch adsorption tests were performed in 250 ml Erlenmeyer flasks shaken in a shaking water bath (HST-205SW at 120 rpm) at a standard temperature of 25 °C to eliminate lead Pb (II) ions from various aqueous solutions.

2.3.1 pH Optimization

The pH of the various solutions was varied from 3 to 8 to figure out the impact of pH on the metal binding of Tl raw fiber and Tls treated fiber. The pH of the solutions was modified to the level needed using 0.1 M HNO_3 and 0.1 M NaOH. The optimal pH for lead ions was determined using solutions with initial concentrations of 10 mg L^{-1} of lead ions and 0.1 g of adsorbent.

2.3.2 Reaction Time Optimization

100 ml of a 10 mg/l solution of Pb^{2+} was used for the adsorption studies, and the contact duration ranged from 5 to 180 min. An atomic absorption spectrophotometer was used to measure the amount of Pb (II) that was still present after adsorption for a specific reaction time.

2.3.3 Optimization of Pb²⁺ Initial Concentration

With an initial Pb (II) ion concentration varying from 10 to 80 mg L⁻¹, batch tests were carried out with 0.1 g of adsorbent and a reaction period of 180 min. The following equation was used to establish the balance of the metal adsorption capacity:

$$Q \left(\frac{\text{mg}}{\text{g}} \right) = (C_0 - C_f) \times \frac{V}{m} \quad (1)$$

where V is the volume of the solution utilized (L), m is the mass of the adsorbent used, Q is the amount of lead adsorbed (mg/g), C₀ is the starting concentration of Pb²⁺ (mg/L), C_f is the equilibrium concentration of Pb²⁺ in the solution (mg L⁻¹), and so forth [11]. The following equation was used to determine the removal efficiency of Pb (II) ions (R%) by both types of media in the aqueous solution:

$$\% \text{ Removal} = \frac{(C_0 - C_f)}{C_0} \times 100 \quad (2)$$

2.4 Adsorption Isotherm

For optimizing its application, isotherms are crucial for understanding the mechanism of the adsorbate-adsorbent interaction. Adsorption isotherms are among the most crucial pieces of information for understanding how an adsorption works, and mathematical analysis of isotherms is required before interpreting the kinetics of an adsorption phenomena. Additionally, finding the ideal correlation for the equilibrium isotherms is essential for optimizing the design of a high absorption unit to eliminate trace metal ions from industrial effluent.

2.4.1 The Langmuir Isotherm

The most popular isotherm for adsorption analysis in latest years is the Langmuir isotherm model, which is employed to explain monolayer adsorption on the surface of an adsorbent with a limited number of identical sites.

The Langmuir isotherm model is expressed linearly as Eq. (3):

$$\frac{C_e}{Q_e} = \frac{1}{Q_{\max} \cdot K_L} + \frac{C_e}{Q_{\max}} \quad (3)$$

Where C_e (mg L⁻¹) stands for equilibrium concentration, q_e for equilibrium metal ion adsorption capacity, q_{max} for maximum adsorption capacity, and K_L for Langmuir equilibrium constant. q_{max} and K_L are determined as a result of the discovery that a graph from C_e/q_e to C_e is a straight

line with an intersection of 1/q_{max} and a slope of 1/K_L·q_{max}. The separation factor, abbreviated R_L, is a dimensionless constant that can be used to explain another crucial aspect of the Langmuir isotherm.

$$R_L = \frac{1}{1 + K_L \cdot C_0} \quad (4)$$

where C₀ denotes the initial Pb (II) concentration (10 mg L⁻¹). According to the value of R_L, the type of isotherm is one that is unfavorable while R_L > 1, linear if R_L = 1, and favorable when 0 < R_L < 1. For the raw *Tl* fiber and the treated *Tls* fiber, the computed R_L values were 0.046 and 0.118, respectively, demonstrating that the adsorption of Pb (II) was a favorable phenomenon. Table 3 compares the maximal monolayer Pb (II) ion adsorption capacity on several chemically treated and untreated adsorbents generated from various precursors.

2.4.2 The Freundlich Isotherm

To determine the proper isotherm needed for the adsorption of Pb (II) from simulated wastewater onto the raw *Tl* fiber and the treated *Tls* fiber, the Freundlich and Langmuir models were utilized. A key requirement of the favorable isotherm is a monolayer sorption with an energy distribution of the active sites that is heterogeneous, combined with an interaction between the molecules that are adsorbed. The Freundlich isotherm is presented as follows:

$$qe = K_F C_e^{1/n} \quad (5)$$

By calculating the values K_F and n using logarithms, the parameters can be linearized:

$$\ln(Q_e) = \ln K_F + \frac{1}{n} \cdot \ln(C_e) \quad (6)$$

where C_e (mg L⁻¹) stands for the equilibrium concentration, Q_e (mg g⁻¹) for the capacity of metal ions to be adsorbed at equilibrium, K_F (mg g⁻¹) and n are constants that characterize the adsorption capacity and intensity, respectively [7]. A straight line is generated by plotting Ln(qe) vs Ln (C_e), and K_F and n can be determined from the intersection and slope, accordingly.

In a water bath heated from 25 to 65 °C, the impact of temperature (T) on Pb (II) adsorption was investigated. While developing an adsorption mechanism, crucial factors such a variation in reaction should be kept in mind. According to thermodynamics, entropy change acts as the primary driving factor in an isolated system when energy cannot be obtained or lost from the environment [3]. Therefore, to determine spontaneous occurrences in environmental engineering practice, both energy and entropy components must be taken into account.

2.5 Kinetic Models

2.5.1 Pseudo-First Order Model

The Lagergren equation represents the pseudo-first order model, which presumes that the ratio of occupied to vacant adsorption sites is proportionate.

$$\frac{dq_t}{dt} = K_1(q_e - q_t) \quad (7)$$

Integrate Eq. (7) for initial conditions $q_t=0$ at $t=0$, Eq. (8) is how the model is obtained in its linearized form.

$$\log(q_e - q_t) = \log(q_e) - \left(k \cdot \frac{1}{2.303}\right)t \quad (8)$$

Where q_e , q_t are the amounts of Pb (II) adsorbed (mg g^{-1}) on the Tl and Tls resin at equilibrium and any instant t , k_1 (min^{-1}) is the rate constant of the pseudo-first-order model, and t is time (min). The $\log(q_e - q_t)$ is drawn as a function of t ; the gradient and intercept are used to calculate k_1 and q_e [8].

2.5.2 Pseudo-Second Order Model

According to the pseudo-second order model, the ratio of loaded to vacant adsorption sites is related to the occupancy rate of those sites. Following are some ways to express the second order kinetic model:

$$\frac{dq_t}{dt} = K_2(q_e - q_t)^2 \quad (9)$$

Integrate Eq. (9) for the starting circumstances: as stated in Eq. (10) provides the linear form at $t=0$ and $qt=0$:

$$\frac{t}{q_t} = \frac{1}{(k_2 \cdot q_e^2)} + \left(\frac{1}{q_e}\right)t \quad (10)$$

In which k_2 is the equilibrium rate constant of the pseudo-second order model ($\text{g} \cdot \text{mg}^{-1} \cdot \text{min}^{-1}$). The q_e and k_2 values are found from the gradient and intercept of the graph of (t/q_t) versus t , respectively.

2.6 Thermodynamic Study

The following equations were used in this investigation to describe how temperature affected the adsorption of Pb (II) by Tl crude and Tls treated resin. The thermodynamic parameters used were the change in Gibbs free energy (G°), enthalpy change (H°) and entropy change (S°) using the following equations:

$$K_c = \frac{Q_e}{C_e} \quad (11)$$

$$\Delta G_{ads} = \Delta H_{ads} - T\Delta S_{ads} \quad (12)$$

$$\Delta G_0 = -RT \cdot \ln K_c \quad (13)$$

$$\ln(K_c) = \frac{\Delta S^0}{R} + \frac{\Delta H^0}{RT} \quad (14)$$

C_e is the quantity of Pb (II) adsorbed on the Tl raw or Tls treated fiber of the fiber at equilibrium (mg L^{-1}) and K_c is the distribution coefficient of biosorption. C_e is also the equilibrium concentration of Pb (II) ions in solution (mg L^{-1}). R is the gas constant, and T is the solution's temperature (K). $\ln(K_c)$ vs $1/T$ van't Hoff graphs' gradient and intersection were used to determine H and S [9].

2.7 Desorption and Reuse of Adsorbents

The Pb^{2+} ion solution (10 mg L^{-1}) was added, and the adsorbents were agitated for 180 min. These Pb (II)-loaded adsorbents were then added to 100 ml of EDTA (0.1 M) solution, where they underwent three cycles of sorption and desorption in succession. The following equation was used to calculate the desorption rate:

$$\text{desorption\%} = \frac{C_e - C_d}{C_e} \times 100 \quad (15)$$

2.8 Statistical Modelling

The use of mathematics to predict trends is called statistical modelling. SMR can improve biosorption processes when several individual factors affect removal efficiency. Based on the experiments, this work determined the best experimental variables for SMR. These were the extraction solution's pH (A), support mass (B), and initial Pb^{2+} concentration (C). Additionally, their interdependent relationship has an impact on how effectively the two carriers, Tl and Tls, remove Pb^{2+} .

The design of an experiment using Design Expert software led to the choice of experimental variables. Each experiment involved a biosorption process using BBD, and the results were reflected in Design Expert version 13. The initial results show three labelled sub-results with run values 1, 0, and -1, consisting of 17 trials that were generated to maximize the biosorption of Pb across three levels of data collecting (II). These tests were all carried out at 25°C . Second order quadratic polynomial equations provide the accurate statistical analysis of the experimental results [12] which describes as:

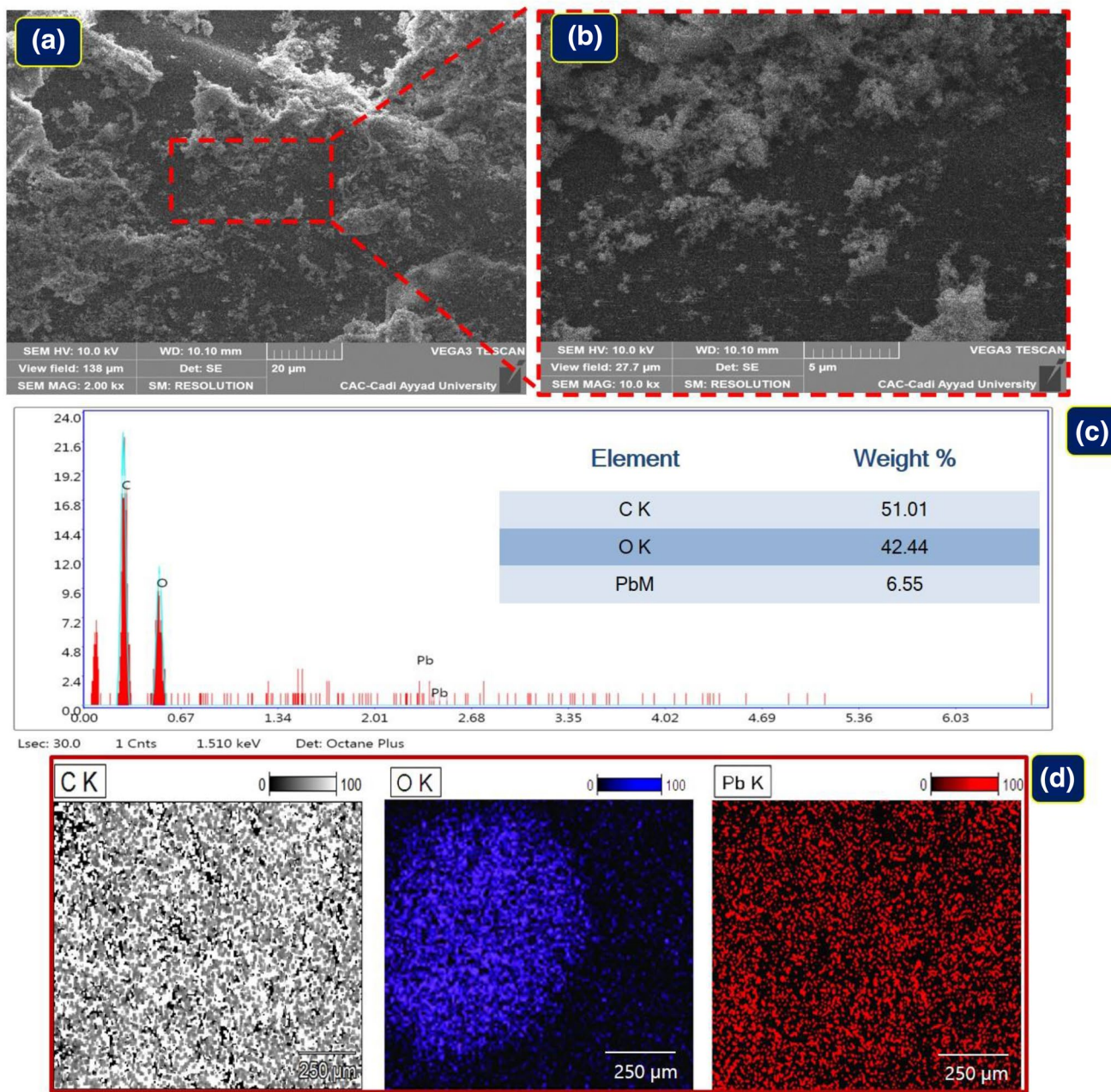


Fig. 1 SEM images of the purified (*Tl*) **a, b** fibers after the adsorption of Pb (II). And EDX images of the purified (*Tl*) **c** fiber after the adsorption of Pb (II) and **d** EDX-mapping micrographs of *Tl* surface

$$R(\%) = \alpha_0 + \sum_{i=1}^3 \alpha_i X_i + \sum_{i=1}^3 \alpha_{ii} X_i^2 + \sum_{i < j} \alpha_{ij} X_i X_j \quad (16)$$

In Eq. (3), R (%) stands for the lead extraction efficiency like a response; a corresponds to the independent factors that were chosen; and a0 (intercept), ai (linear effect), aii (quadratic effect), and aij (interaction effect) indicate the model coefficient values. The model coefficients a_{ij}, a_{ii}, a₀, a₁, a₂ and a₃ are found in Eq. 16. Their names refer to the order in

which they appear in the model. A refers to the lead removal efficiency, which is represented by R (%) in the equation. Various aspects of the significance of the quadratic equation were assessed by ANOVA analysis. This includes the evaluation of the R² and no-fit coefficients, which are used to examine the fit of the predicted model. Another method of assessing significance was by regression, which resulted in the determination of R² and no-fit [13]. Design Expert software was used to create 3D models for the *Tl* and *Tls* media. This resulted in the creation of a graphical representation

correlating the p-values of the variables studied at a significance level of $p < 0.05$. This led to the creation of optimal conditions for lead bio sorption, as well as the effects of changing these conditions.

3 Results and Discussion

3.1 Characterization of the Adsorbent

3.1.1 Surface Morphology

The Fig. 1 depicts the microstructures of the fibers both before and after the acid treatment. After analyzing the SEM images, it was easy to see the differences between the surface morphology of the reed fibers before and after the acid treatment. After the treatment, there was a noticeable

alteration in the adsorbents' surface. Particularly, the reed fiber's surface before the acid treatment primarily comprised of flat multilayers [8]. With the acid treatment, there seemed to be more pores on the fiber, suggesting that the acid treatment can vastly enhance pore volume and may also help boost the ability of Pb (II) ions to bind to the fiber's surface.

The EDX diagrams (Fig. 2) are present in spending (*Tl* and *Tls*). Firstly, residues may be eliminated by washing the support in HCl acid as shown in Fig. 2. The notion of electron-matter interactions is the foundation of the microscopy technique known as scanning electron microscopy (SEM). Scanning electron micrographs of the adsorbent's exterior vividly show its morphology and texture, Fig. 1. The external morphology of the surface of raw fiber (*Tl*) is different from that of the bark treated with sulfuric acid (*Tls*). After being processed sulfuric acid *Tls* has a very irregular structure and more porous than the crude bark, and therefore

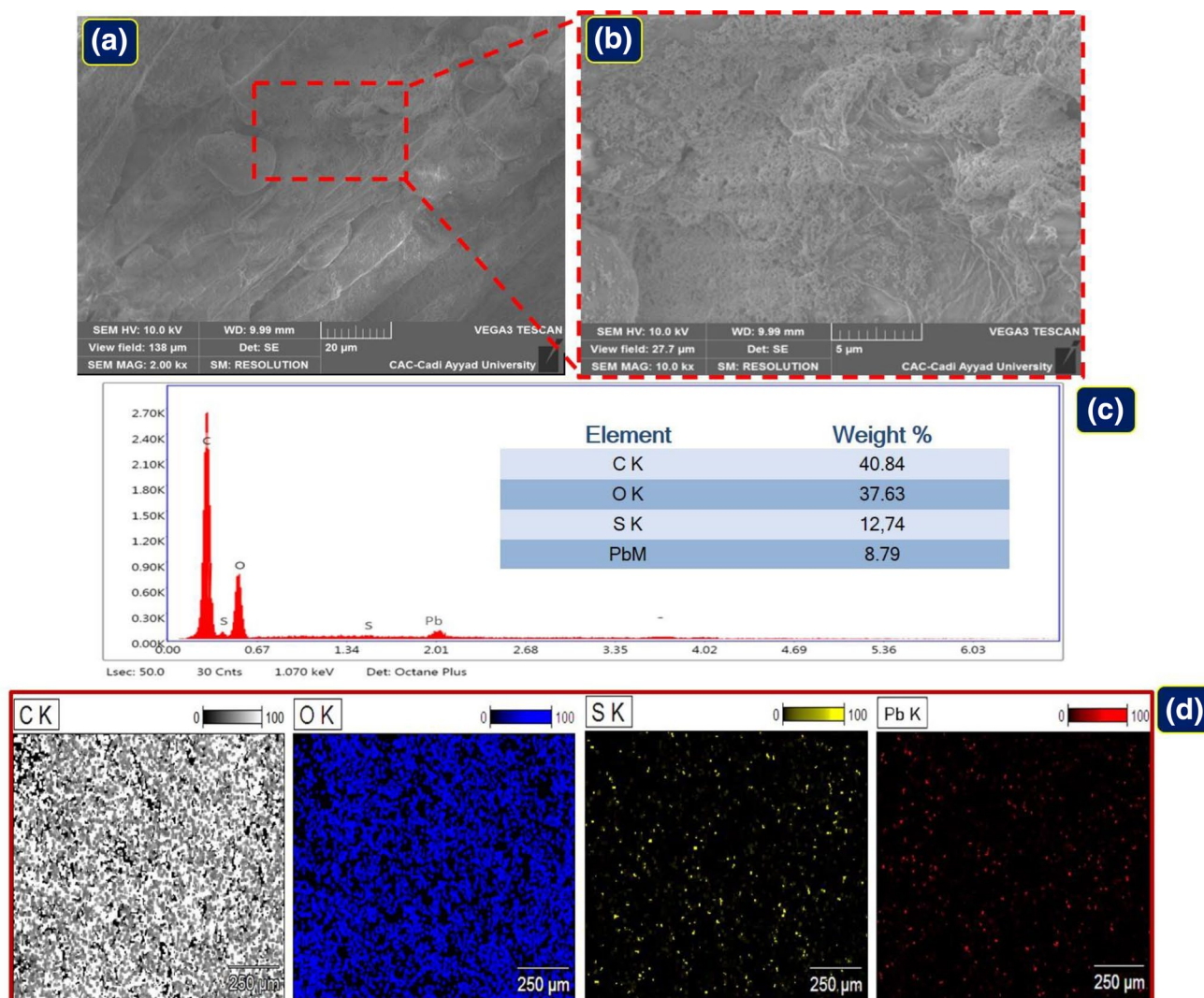


Fig. 2 SEM images of the purified (*Tls*) **a**, **b** fibers after the adsorption of Pb (II). And EDX images of the purified (*Tls*) **c** fiber after the adsorption of Pb (II) and **d** EDX-mapping micrographs of *Tls* surface

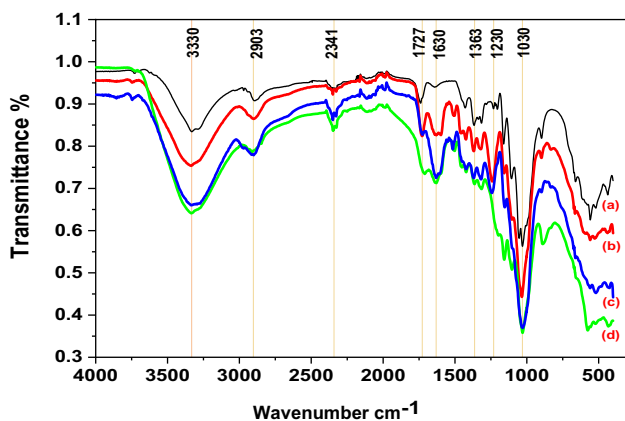


Fig. 3 FTIR spectra of fibers *Tl* (a, b), *Tls* (c, d) resin before and after Pb^{2+} adsorption

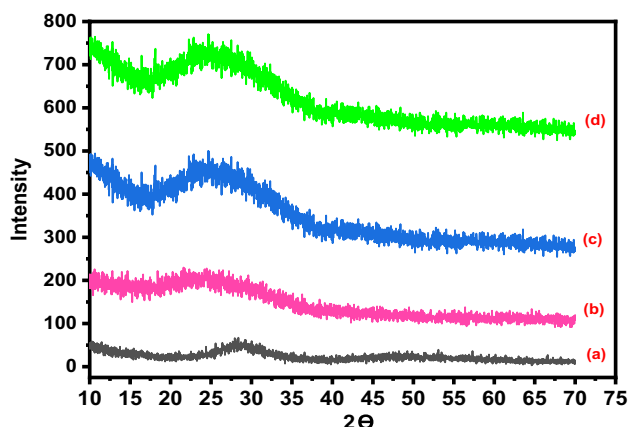
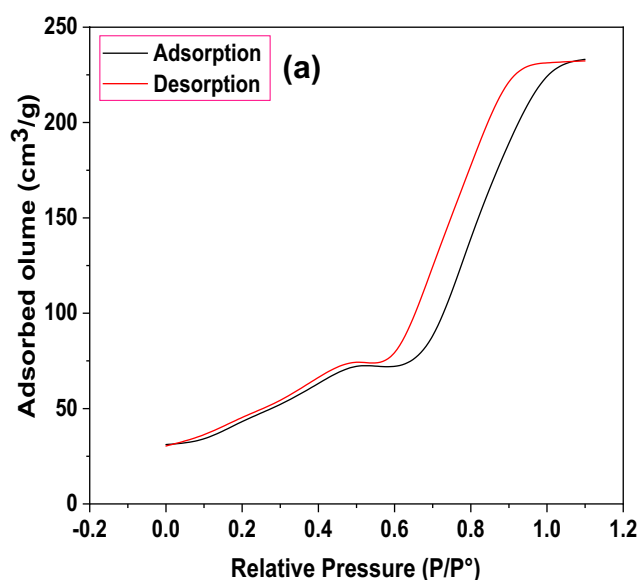


Fig. 4 X-ray diffraction curves of raw (a, b) and activated (c, d) fibers before and after adsorption



a larger specific surface area, justifying better adsorption capacity. SEM of adsorbent bios (*Tl*, *Tls*) after extraction of Pb (II). Indeed, after adsorption of metals, a change in the structure of the barks was observed and they seem to have a rough surface of the pores because they are partially covered by the metal ions Fig. 2. Show the EDX spectra before and after adsorption of Pb (II) ions. EDX clearly shows the adsorption of Pb (II) metal ions on all the supports studied [14].

3.1.2 Infrared Spectra Analysis

Different chemical functionalities were attributed to distinctive vibration bands in conformity with the scientific literature. Although the FTIR spectra of *Tl* and *Tls* were practically identical, the density of the soda-treated shell was higher.

The infrared spectra of inactivated (*Tl*) and activated (*Tls*) fibers are shown in Fig. 3. Bands related to the (S=O) and (SO₃H) bands respectively occur at 1625 and 1236 cm^{-1} as a result of partial *Tls*. There are considerable amounts of sulfate esters, which are identified by three bands at 2350, 1360, and 600 cm^{-1} . (According to the number of free sulfates determined from sodium sulfate). Yet, this method does not enable the distinction between N- and O-sulfates. However, because primary amines are more reactive than primary alcohols, O-sulfate groups and N-sulfate groups could build in order to account for the minute quantity of chitin found in our resin [15].

If there is an impact of chemical pre-treatment and metal biosorption on the functional groups, the proper

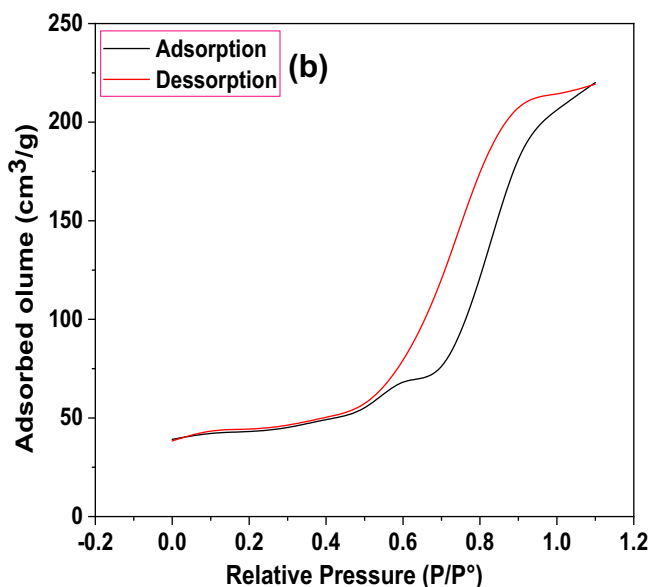


Fig. 5 Adsorption and desorption isotherm of N_2 at 77.3 K on the surface of three materials a *Tl* and b *Tls*

explanation of a change in the spectra, the decrease and disappearance of peaks can be utilized [16]. In order to ascertain the interactions between the functional groups and the Pb (II) ions, the FTIR spectra of the lead (II)-loaded fiber and the treated lead (II)-loaded fiber were compared. As seen in Fig. 3, the presence of the OH stretching vibration is indicated by peaks at 3323 cm^{-1} . There were other peaks at 2888 (OH stretching of the carboxylic acid), 1735 cm^{-1} (C=O in the carboxylic acids and carboxylates), 1373 cm^{-1} (N–O), 1232 cm^{-1} (carbonyl), and 1030 cm^{-1} (C–O). In comparison to the *Tl* crude fibers, the lead (II) loaded fibers had some elongation shifts at 3323 , 1735 , 1630 , and 1232 cm^{-1} . There were a few little peaks visible in the Pb (II) loaded fiber that occurred at 1630 cm^{-1} . The alterations that followed sorption may be a sign that metal binding processes happened on the *Tls* active sites. Since the FTIR spectra of the Pb (II)-loaded fiber and the modified Pb (II)-loaded fiber do not significantly differ from those of the raw fiber, it can also be inferred that physisorption was the primary mechanism [14].

3.1.3 X-Ray Diffraction Measurements

The fiber is made up of amorphous polymers (hemicelluloses and lignin) and polymers organized, in places, in crystalline zones (cellulose). It has been shown that the amorphous areas of cellulose are more sensitive to chemical and enzymatic attacks than the crystalline areas. Figure 4 displays the X-ray diffraction patterns of the unmodified and modified fiber samples prior to and after adsorption [10].

It appears that the filter was affected by the treatments used, where the crystallinity index of the fiber treated with sulfuric acid increased under the effect of the crosslinking of the cellulose from 0.35% for the 6.47% raw fiber (*Tl*) for the filter activated with sulfuric acid (*Tls*). This increase is due to the reaction of OH groups in cellulose with sulfuric acid [17]. As a consequence, their hydrogens can no longer be used to create intermolecular hydrogen bonds, which causes cellulose to lose a little of its crystal structure (Fig. 5). In addition, there is a slight increase in the crystallinity index for the acid-treated filter (*Tls*) (45.87%), this increase is due to the loss of extractables (amorphous) [18].

3.1.4 Specific Surface

The results of the adsorption–desorption isotherms of the biomaterials are recorded in Table 1. In this table, we have recorded the texture parameters of the biomaterials: the nature of the samples, the BET surface area ($S_{\text{BET}}\text{ m}^2\text{ g}^{-1}$), the microporous volume ($V_{\text{mic}}\text{ cm}^3\text{ g}^{-1}$) and the mesoporous volume ($V_{\text{mes}}\text{ cm}^3\text{ g}^{-1}$).

Table 1 Specific surface areas of the different materials

Material	Specific surface area ($\text{m}^2\text{ g}^{-1}$)	Microporous volume ($V_{\text{mic}}\text{ cm}^3\text{ g}^{-1}$)	Mesoporous volume ($V_{\text{mes}}\text{ cm}^3\text{ g}^{-1}$)
<i>Tl</i>	1.784	0.11	0.12
<i>Tls</i>	3.037	0.17	0.23

From these results it can be observed that the BET surface areas of *Tls* are higher than those of *Tl* raw materials. This is due to the chemical treatment which has a great effect on the textural properties of the adsorbents, and the adsorption properties of the materials depend primarily on their surface chemistry. After activation of *Tl* by H_2SO_4 , the surface areas increase significantly. They increase from 1784 to $3037\text{ m}^2\text{ g}^{-1}$ for *Tls*, respectively, which are important surface areas for adsorption processes. All the studied biomaterials are more or less microporous, the microporous volume of *Tls* from H_2SO_4 activation is the largest $0.11\text{ cm}^3\text{ g}^{-1}$ which indicates that *Tls* is a microporous adsorbent, the mesoporous volume represents $0.23\text{ cm}^3\text{ g}^{-1}$ for *Tls*, the acid activation indicates that these materials have a mesoporous structure.

3.1.5 Thermal Stability

The application of microfibers as additional reinforcement in bio-composites is significantly influenced by their thermal properties. The derived thermogram analysis (DTG) and thermogravimetric analysis (TGA) curves for the untreated and treated materials, respectively, are shown in Fig. 6 [19]. The TGA curves demonstrate a preliminary weight loss of less than $155\text{ }^\circ\text{C}$; this preliminary loss (6.5% for the raw sample and 4.5% for the modified microfibers) is attributed to the evaporation of surface-bound moisture, chemisorbed water bound to the samples' interiors, and/or low molecular weight compounds like extractible present in the raw sample. The existence of the absorbed water has initially been confirmed by FT-IR results. The principal and most significant thermal degradation of cellulose (50.84%) takes place above $179\text{ }^\circ\text{C}$ and includes a number of simultaneous mechanisms such as dehydration, depolymerization, and glycoside unit degradation.

The unprocessed example demonstrated distinct pyrolysis procedures above a larger temperature range, such as thermal depolymerization of hemicellulose up to $273\text{ }^\circ\text{C}$, cellulose degradation up to $348\text{ }^\circ\text{C}$, and lignin degradation up to $536\text{ }^\circ\text{C}$, in addition to its simultaneous decomposition with other degradation procedures because of its complex structure. For the untreated and treated samples, respectively, the DTG curves exhibited maximal degradation rates at $\text{DTG max} = 354\text{ }^\circ\text{C}$ and $341\text{ }^\circ\text{C}$. The peak that can be evidently seen at around $391\text{ }^\circ\text{C}$ on the left side of the principal peak

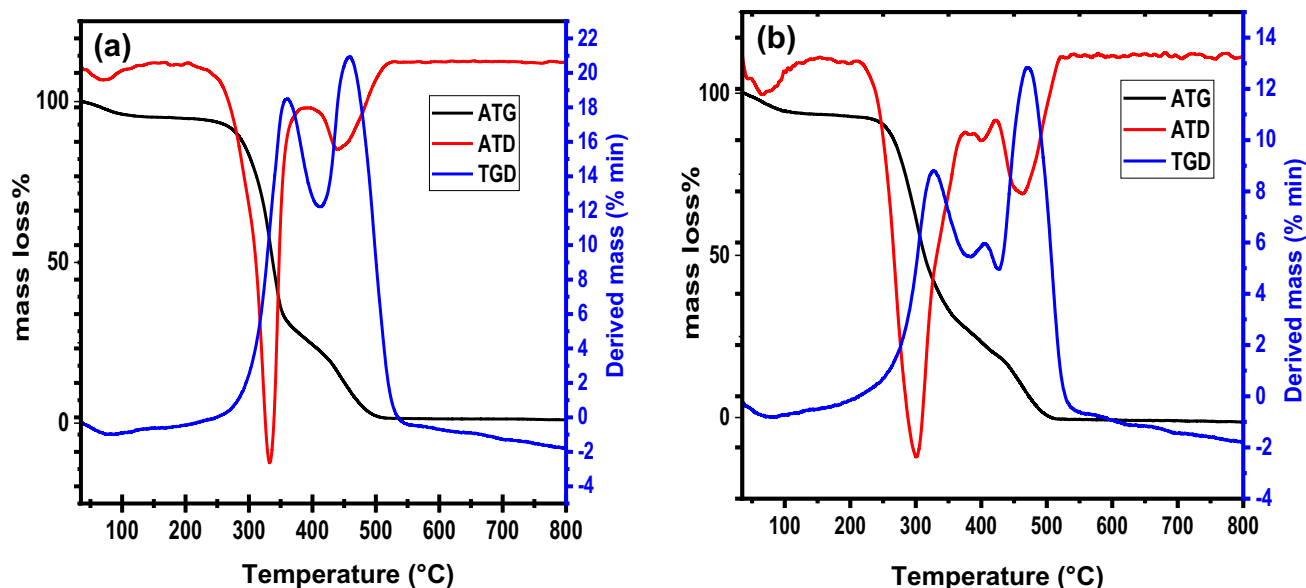


Fig. 6 Thermogravimetric and differential analysis curves of raw *TI* (a) and activated *TIs* (b) microfibers.

of the DTG curve of the treated sample is a result of the principal deterioration of the hemicellulose and non-cellulosic elements, as opposed to the widening at 425 °C on the ATD curve of the microfibers, which may be a sign of a broad molecular weight distribution of cellulose or residual hemicellulose content that withstood the processing procedure. In the end, a carbonized deposit was created (42% for the untreated microfibers and 46% for the treated sample). Because non-cellulosic elements have the ability to enhance carbon synthesis, there is more carbonized residue in the raw sample than there is in the processed sample. Since the cellulose microfibers from reed fiber generated a relatively high amount of char when compared to the literature, this suggests that a greater amount of non-volatile carbonaceous material was generated during pyrolysis and could be indicative of the treated microfibers' high thermal stability [20].

3.2 Adsorption Characteristics

3.2.1 Effect of Contact Time

We introduced 0.1 g of the reed filter to 100 ml of a $\text{Pb}(\text{NO}_3)_2\text{-H}_2\text{O}$ solution at a concentration of 10 ppm for 180 min in order to test the effects of the contact time between the lead (adsorbate) in solution and the resin (adsorbent). The results are shown in Fig. 7. [10]. $\text{Pb}(\text{II})$ ions are weakly retained on the resin; a maximum efficiency of 77.68% is recorded for a contact time of 60 min. This explains the low affinity of the support (*TIs*) for $\text{Pb}(\text{II})$ ions. These findings show that this material's ability to retain lead ions is not very effective. After that, we continued with a

chemical process to increase its adsorption capacity [21]. We note that the adsorption rate increases rapidly with increasing mass of the modified fibers (*TIs*). For a 40-min contact period, a yield of more than 96% is attained. Approximately 98% efficiency remains after 60 min.

3.2.2 Optimization of the Adsorbent Mass

We conducted the experiment under the following operating circumstances in order to find the ideal mass of the adsorbent: A specific mass of the adsorbent, ranging from 0.02 to 0.8 g, is in contact with 100 ml of $\text{Pb}(\text{NO}_3)_2(\text{H}_2\text{O})_5$ solution, which has a concentration of 10 ppm. The solution is filtered after 180 min of agitation, and the remaining $\text{Pb}(\text{II})$ concentration is calculated. Figure 8 displays the study's outcomes. The mass of the modified *TIs* has an effect on the adsorption effectiveness, as we have noted [22]. The optimal rate is recorded for a mass of 0.1 g, the rate reached remains almost the same, with quantities from 0.02 to 0.8 g. The continuous rate increased slightly for the 10-ppm concentration. This may be explained by the quantity of $\text{Pb}(\text{II})$ is removed from the solution [23].

3.2.3 Optimization of $\text{Pb}(\text{II})$ Concentration

We used $\text{Pb}(\text{NO}_3)_2(\text{H}_2\text{O})_5$ solutions with varying concentrations from 10 to 100 mg L^{-1} to test the pollutant's ability to adsorb on the *TI* and activated *TIs* with the optimized mass of 0.1 g. Figure 9 displays the calculated yields as a function of $\text{Pb}(\text{II})$ concentration. It should be noted that when concentration rises, $\text{Pb}(\text{II})$ ion retention rates on the adsorbent

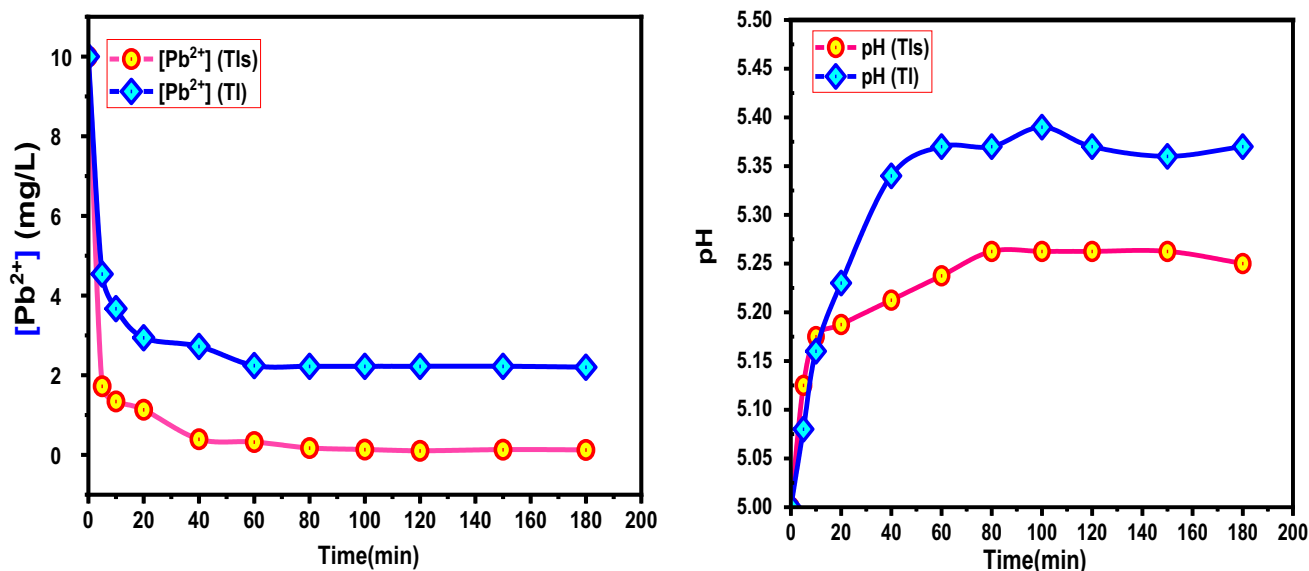


Fig. 7 The stirring time on the $[Pb(II)]$ and the pH change by the (Tl) and (Tls) fiber. $[Pb^{2+}] = 10 \text{ mg L}^{-1}$, $m = 0, 1 \text{ g}$, $V = 100 \text{ ml}$, $pH_i = 5$, $t = 3 \text{ h}$ and $T = 298 \text{ K}^\circ$

change gradually. For a concentration of 10 mg L^{-1} , a yield of nearly 100% for Tls and 78% for Tl is recorded. Above this point, a decline in the rate is seen and it drops to about 59% Tls and 36% Tl for a concentration of 40 mg L^{-1} . This can be attributed to the adsorbent becoming saturated at high metal ion concentration levels [24].

3.2.4 pH Optimization

We continued as previously, keeping the metal concentration at 10 ppm, the mass of the adsorbent at 0.1 g, and adjusting

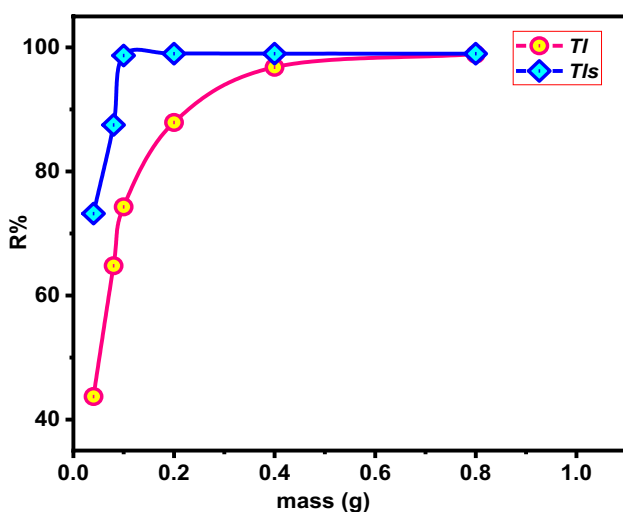


Fig. 8 Effect of mass on extraction efficiency. $[Pb^{2+}] = 10 \text{ mg L}^{-1}$, $V = 100 \text{ ml}$, $pH_i = 5$, $t = 3 \text{ h}$ and $T = 298 \text{ K}^\circ$

the pH in the range of 3 to 8 pH units [25]. This allowed us to establish the ideal pH value that would enable the optimum retention of Pb (II) ions on our resin. The findings given in Fig. 10 reveal that pH significantly affects the Pb (II) ion's ability to bind to the raw and modified resin. Indeed, the increase of the pH value from 3 to 7 induces an increase of the adsorption efficiency from 65% to about 77% for the raw fibers (Tl), and from 78 to 98% for the activated fibers (Tls). The results obtained are shown in Fig. 10 [26]. We can deduce that neutral and acidic pH is more favorable for this operation. This may be related to the surface charge of activated Tls, which contains many OH groups, which are available to release H^+ protons at acidic pH, to

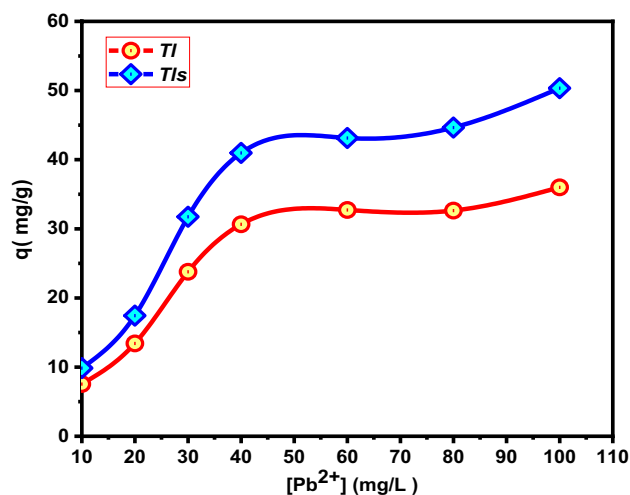


Fig. 9 Effect of initial Pb (II) concentration on the capacity of (Tl), and (Tls). $m = 0, 1 \text{ g}$, $V = 100 \text{ ml}$, $pH_i = 5$, $t = 3 \text{ h}$ and $T = 298 \text{ K}^\circ$

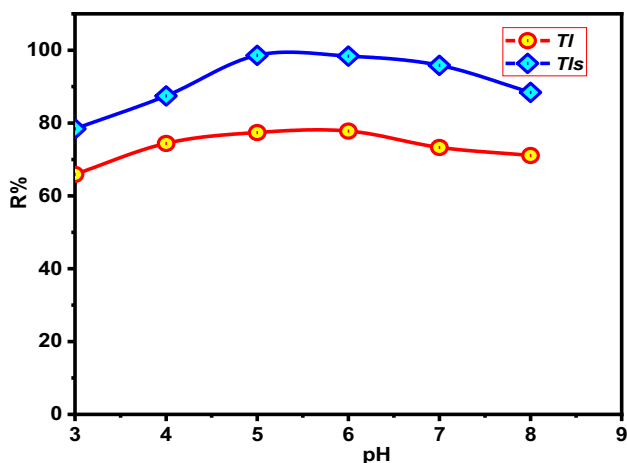


Fig. 10 Effect of initial pH on the extraction efficiency of Pb (II) by *Tl*, *Tls*. $[Pb^{2+}] = 10$ ppm, $m = 0$, 1 g, $V = 100$ ml, $t = 3$ h $T = 298$ K $^\circ$

give O-groups that are favorable for the binding of Pb^{2+} ions, carrying the same type of charge (there will be competition).

3.2.5 Effect of Temperature

The effect of temperature on the extraction of Pb (II) by *Tl* and *Tls* fibers are studied at temperatures 25, 35, 45, 55, 65 $^\circ$ C. For this study, the agitation of the aqueous phase-resin mixture is ensured by magnetic agitation on a water bath in order to control the temperature. The results obtained are shown in Fig. 11.

An increase in the hydrophobicity of the resin with heating, a swelling of the resin which increases the size of the

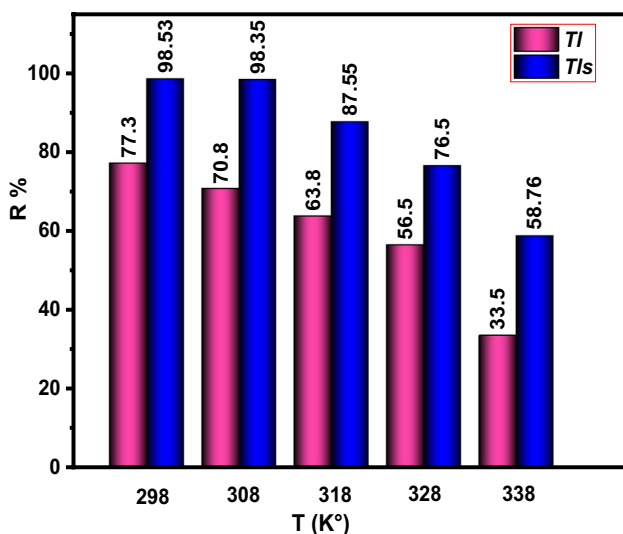


Fig. 11 Effect of temperature on the extraction efficiency of Pb (II) by *Tl* and *Tls* fibers. $[Pb^{2+}] = 10$ ppm, $m = 0$, 1 g, $V = 100$ ml; $pH = 5$, $t = 3$ h

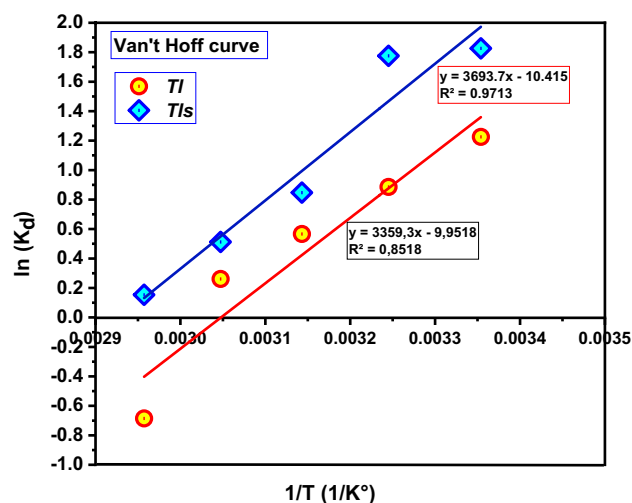


Fig. 12 Van't Hoff curve for Pb (II)

pores and cavities thus making it easier to release the Pb (II) ions which were trapped in the resin in the aqueous phase, a greater mobility of the ions which will prevent them from adsorbing better on the surface of the resin, and the destruction of the resin by rubbing with the magnetic bar changes the morphology of the resin (porosity and specific surface) [27].

3.3 Thermodynamic Study

The adsorption of Pb (II) on both resins was favorable and spontaneous, as evidenced by the fact that the free energy change (G) measured during the adsorption reaction at temperatures ranging from 25 to 65 $^\circ$ C were all negative (Figs. 12, 13). Moreover, as temperature rose, the free energy variation dropped (Table 2). The Pb (II) adsorption process was confirmed to be exothermic by the negative value of enthalpy change (H°), and this behavior suggested that the adsorption process was more favorable at low temperatures. Following Pb (II) adsorption on *Tl* and *Tls*, the variation in entropy (S°) has a negative value, reflecting a reduction in randomness at the solid/solution interface [28].

3.4 Adsorption Isotherms

At a temperature of 20 $^\circ$ C, isothermal experiments were conducted using a range of Pb (II) concentrations (10–1000 mg/L). The Langmuir and Freundlich isotherms were chosen to be employed in this research to replicate two widely utilized models.

The Freundlich and Langmuir adsorption isotherms are illustrated in Fig. 14a and b, respectively. Table 3 lists the R^2 values for the Freundlich constants n and K_F , the Langmuir constants K_L and q_{max} , and the associated correlation

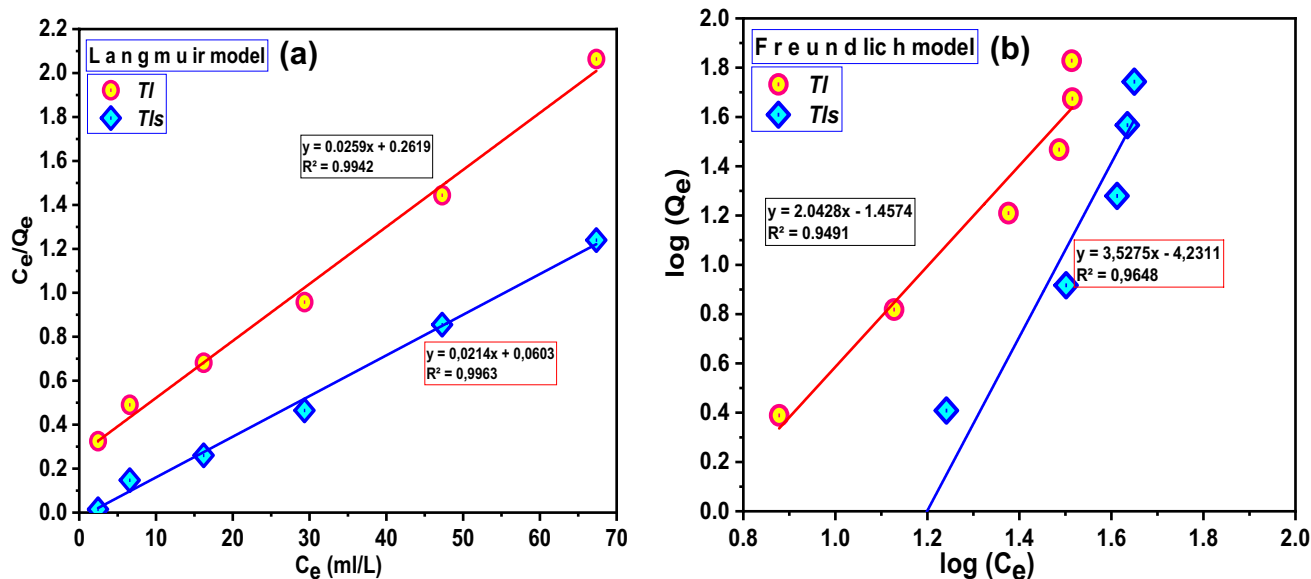


Fig. 13 Linear form of the Langmuir (a) and Freundlich (b) model of Pb (II) on both fibers

Table 2 Thermodynamic parameters of Pb (II) adsorption on the two supports

Adsorbent	T(K)	LnKd (L g ⁻¹)	ΔH° (KJ mol ⁻¹)	ΔS° (J mol ⁻¹ k ⁻¹)	ΔG° (KJ mol ⁻¹)
<i>Tl</i>	298	1.22	- 27.92	- 82.70	- 3.27
	308	0.88			- 2.44
	318	0.56			- 1.6
	328	0.26			- 0.79
	338	- 0.68			0.03
<i>Tls</i>	298	1.82	- 30.71	- 86.59	- 4.90
	308	1.77			- 4.04
	318	0.84			- 3.17
	328	0.51			- 2.30
	338	0.15			- 1.44

coefficients. For the unprocessed *Tl*s fiber and the processed *Tl*s fiber of the blade filter, respectively, the computed Freundlich constants n was 1.90 and 2.53 [29]. The Freundlich model proved insufficient to capture the equilibrium interactions between the two different types of adsorbents, as shown by the linearized equations' poor correlations for the removal of Pb (II) ions from the two adsorbent types. According to Langmuir isotherm plots, the coefficients of determination (R^2) and q_{max} values for *Tl* and *Tl*s, respectively, were 0.753 and 0.8609 and 31.94 and 46.51 mg g⁻¹. It is evident that the equilibrium data and the Langmuir isothermal model do not match up [30]. It needs to be mentioned that adsorption capacity differs and relies on an individual adsorbent's properties, the degree of surface treatment, the analytical

technique used for decontamination, the processing temperatures, and the initial concentration of the adsorbate utilized. The activated *Tl*s fibers have a respectable adsorption capacity and are the best at removing Pb (II) ions when compared to other comparable chemically treated adsorbents (Table 3).

The correlation coefficients obtained allow us to say that the two isotherms (L and F) model our results well. This indicates that the adsorption takes place in monolayer without interactions between the Pb (II) adsorbate molecules. The maximum adsorbed capacity is given by Q_{max} and is equal to 46.51 mg/g which represents a good capacity for such a material compared to other materials such as ion exchangers. The parameter n ($n=0.9$) of the Freundlich isotherm confirms a considered average adsorption of the adsorbate (Pb (II)) on our adsorbent.

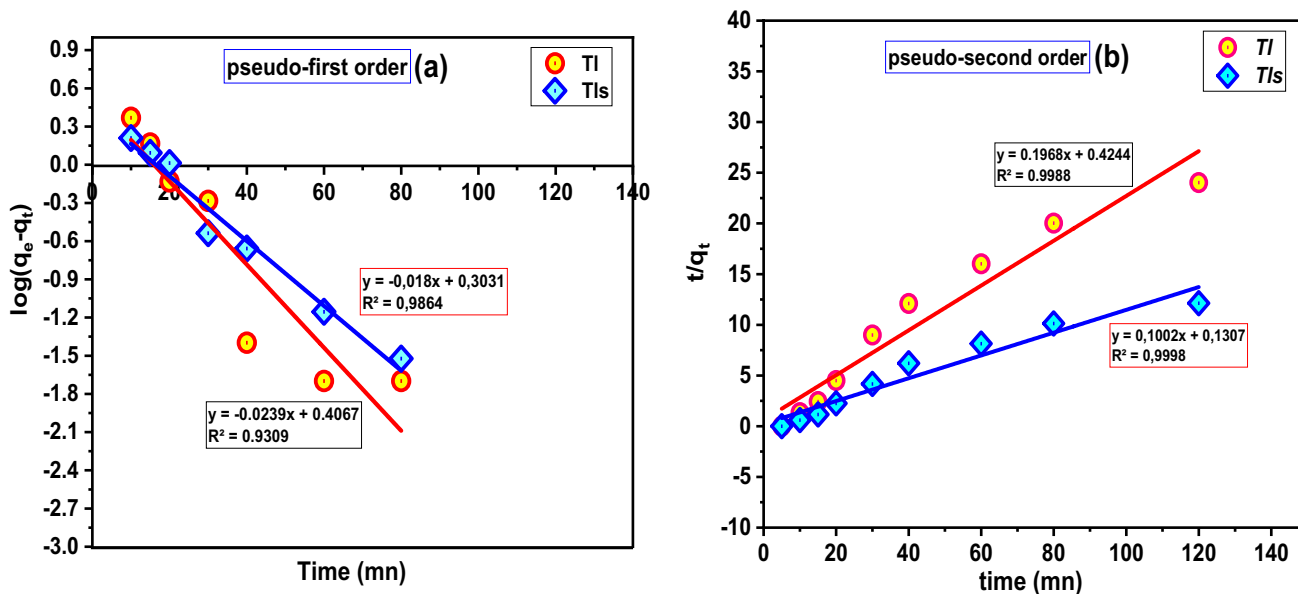


Fig. 14 Pseudo first-order (a) and second-order (b) kinetic models of adsorbed Pb (II)

Table 3 Isothermes de Langmuir et Freundlich pour l’adsorption du Pb (II)

Isotherm	Parameters	Adsorbent	
		<i>Tl</i>	<i>Tls</i>
Freundlich	K_f (mg g ⁻¹)	67.68	85.08
	n	0.81	0.949
	R^2	0.9491	0.9648
Langmuir	Q_m (mg g ⁻¹)	31.94	46.51
	K_L (L mg ⁻¹)	0.046	0.118
	R_L	0.68	0.46
	R^2	0.9942	0.9963

Table 4 Parameters of pseudo-first order and pseudo-second order kinetic model

Isotherm	Parameters	Adsorbent	
		<i>Tl</i>	<i>Tls</i>
Pseudo-first order	$q_{e-calcul}$ (mg g ⁻¹)	2.5	2
	k_1 (min ⁻¹)	0.055	0.0414
	R^2	0.9309	0.9864
Pseudo-second order	$q_{e-calcul}$ (mg g ⁻¹)	5.08	9.98
	k_2 (min ⁻¹)	0.302	0.277
	R^2	0.9988	0.9998

3.5 Kinetic Modelling

In the time range of 5–120 min, the kinetic experiments of Pb (II) adsorption to both *Tl* raw fibers and *Tls* treatments were conducted. It is ultimately possible to establish the solute uptake rate in the kinetic analysis, which establishes the residence time necessary for the adsorption reaction to be completed. The mechanism of the adsorption process was determined using pseudo-first and pseudo-second order models.

Table 3 lists the adsorption kinetic parameters, and Fig. 14 displays the pseudo-first order and pseudo-second order model graphs for Pb (II) adsorption on *Tl* and *Tls* resins. The pseudo-second order kinetic model's correlation (R^2) values for *Tl* and *Tls* resins were 0.9998 and 0.9988, respectively. In comparison, with the modified resin, the correlation coefficients of the pseudo-first order kinetic model

Table 5 Adsorption cost of Pb²⁺ ions by *Tl* and *Tls*

Materials	Capacity mg g ⁻¹	the cost of preparation US\$ kg ⁻¹	The adsorption cost US\$ kg ⁻¹
<i>Tl</i>	32.64	0.07	2.14
<i>Tls</i>	44.65	0.3	6.71

were relatively low than those of the pseudo-second order kinetic model (Tables 4, 5). As a result, it is possible to draw the conclusion that the Pb (II) adsorption system followed a pseudo-second order.

3.6 Proposed Mechanism for Pb²⁺ Removal

The parameters of the adsorbent qualities of the adsorbate (Pb²⁺), involving physical tests and chemical processes,

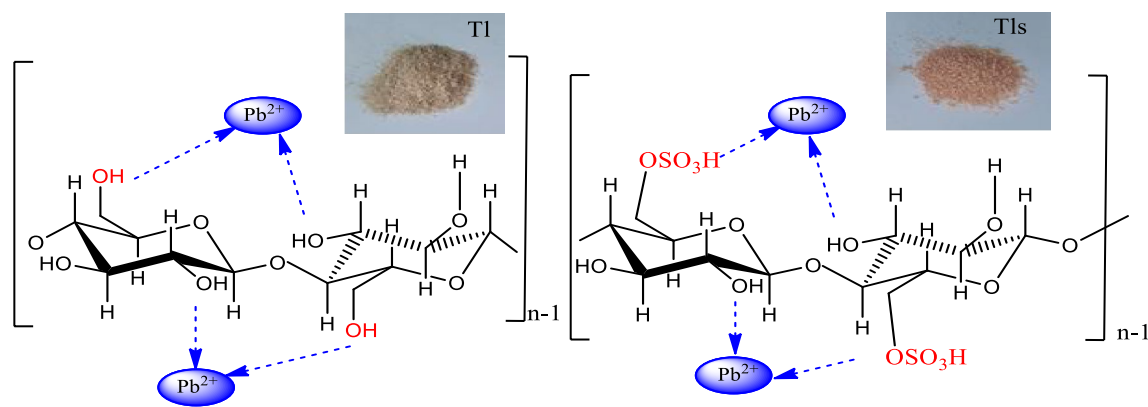
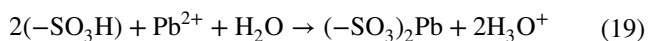
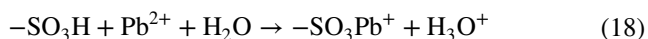
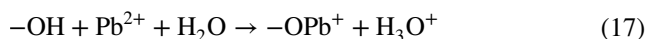


Fig. 15 Possible mechanisms of Pb (II) biosorption by fibers

relied on whether the *Tl* fiber surfaces were acid-treated or not [31]. Pb (II) ion molecules were tightly bound by adsorption forces when they were adsorbed on the adsorbent surface. Numerous functional groups including carbon and oxygen were discovered on the tested adsorbent's surface after a study of the infrared spectra acquired from the adsorbent. Thus, it is probable that an ion exchange process that released protons from the sorbent into the adjacent aqueous medium caused the Pb^{2+} uptake [32].

This was verified by data showing a fall in pH following the addition of Pb^{2+} to an aqueous solution. The following reactions could take place as part of the ion exchange process between H^+ ions and Pb (II) on the biopolymer surface:



The metal exchanges cations with hydrogen ions linked to the sulfonic and hydroxyl groups in these cation exchange processes. Due to these findings, we came to the conclusion that sulfonic and hydroxyl groups are crucial to the process of Pb (II) ion adsorption from aqueous solutions. Matter of fact, numerous reports have shown that this mechanism operates. For example, H_2SO_4 can be used to modify needs to enhance the amount of acidic groups that are present on their surface [33].

According to the proposed reaction mechanism, the chemical mechanism involves the development of a covalent bond, a van der Waals force and an ionic bond between the proton ion and the OH and SO_3H functional groups on the surface of the adsorbent (Fig. 15). The pH of the environment has a significant impact on the electrostatic attraction mechanism. The specific explanation of why the maximum

adsorption of Pb (II) from aqueous solution onto *Tl* and *Tls* occurs at a slightly acidic pH between 5 and 7 can be found in subsection 3.2.4. The anionic charged surfaces of the *Tl* and *Tls* supports at this pH have developed the strongest electrostatic affinity for the positively charged Pb (II) cations. Depending on the nature of the interaction between the adsorbent material and the adsorbate, the adsorbate molecules can be adsorbed on the surface of the adsorbent via physisorption (physical adsorption) or by chemisorption (chemical adsorption) [34]. The process of physisorption is always exothermic and occurs at high intracellular pressures. Most of the action takes the shape of a multilayer. A physisorption process has an adsorption energy of less than 40 kJ mol^{-1} , whereas a chemisorption process has an adsorption energy of more than 40 kJ mol^{-1} . The value of the adsorption energy (variation in enthalpy) for the elimination of Pb (II) ions by biological materials is $-27.92 \text{ kJ mol}^{-1}$ for *Tl* and $-30.71 \text{ kJ mol}^{-1}$ for *Tls*. This indicates that during the adsorption process, the physisorption mechanism predominates [35].

3.7 Pb (II) Regeneration

To properly dispose of and reuse the adsorbent, Pb (II) must be recovered from the loaded adsorbent. The adsorbed Pb^{2+} must be desorbed, and the adsorbent must then be regenerated for more adsorption–desorption cycles, in order to reduce the expenses of the entire recovery process [36]. In this case, EDTA 0.1 M was selected to assess the adsorbents' capability. Figure 16 demonstrates the Pb (II), Pb (II) ions loaded on *Tl*, and *Tls* desorption effectiveness. The desorption efficiency of Pb (II) for *Tl* and *Tls* was 64.42 and 78.21%, respectively, over three successive regeneration (adsorption–desorption) cycles. After three cycles, the Pb (II) ions might be discharged at a recovery level of more than around 78% using recycled adsorbents. The outcome supports the hypothesis that Pb

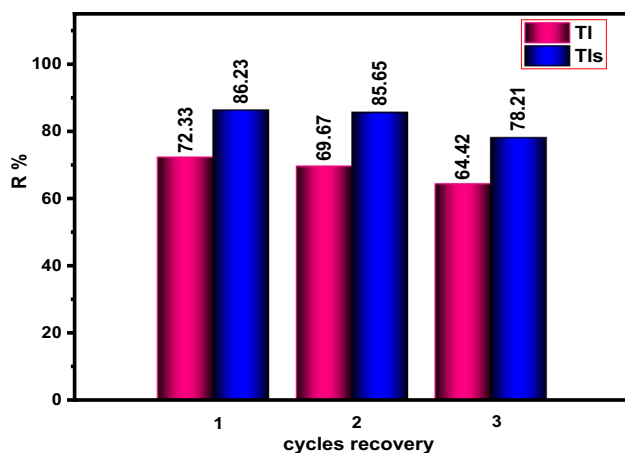


Fig. 16 The Pb (II) desorption efficiency

(II) ions from the aqueous solution could be decreased by the acid-treated reeds [37].

3.8 Evaluation of adsorbents, economic analysis

The reed filters appeared to us to be more interesting from all points of view, both environmental, technical and economic. The advantages of reeds in non-collective sanitation are numerous: raw water system, minimal sludge production that can be used as compost, moderate investment, long-lasting system, maintenance independence.

The effectiveness of adsorbents was examined by an analysis of the adsorption expense for Pb (II) removal. The adsorption capacity of Pb²⁺ ions and the cost of developing the adsorbents were used to determine the expense of the adsorbents [38].

$$\begin{aligned} & \text{Cost of adsorption} \left(\frac{\text{US\$}}{\text{Kg}} \right) \text{Pb(II)} \\ &= \frac{\text{The cost of preparation} \left(\frac{\text{US\$}}{\text{Kg}} \right)}{\text{Adsorption capacity} \left(\frac{\text{mg}}{\text{g}} \right)} \times 100 \end{aligned} \quad (20)$$

The price of the chemicals used in the creation of *TI* and *TIs*, the energy used in the activation procedures, and the cost of the water required (in Morocco) for the cleaning equipment were all taken into consideration. This research did not take into account any expenses related to the waste's disposal. *TI*, *TIs* were 2.14 and 6.71 US dollars kg⁻¹, respectively. The outcome shown that reeds, among the most widely accessible forest wastes in Morocco, can be employed as a practical method to eliminate Pb²⁺ ions from wastewater.

3.9 Comparative study

Biosorbents are by nature heterogeneous materials, therefore the different modifications reported in the literature affect particular chemical functions or classes of molecules. Table 6 reports on some modifications of biosorbents to improve their properties towards lead and cadmium.

The purpose of treatments using organic solvents is to extract specific compounds such as tannins and circulating sugars. Polysaccharides are esterified with carboxylic acids or their derivatives (citric or succinic). They have a double purpose: on the one hand, the presence of several acidic carboxylic functions allows the cross-linking of chains between them, and on the other hand, the presence of several acidic carboxylic functions on the surface increases the number of acidic carboxylic functions. The above table includes

Table 6 Examples of chemical modifications of some biosorbents and their lead and/or cadmium retention capacities

Biosorbent	Treatment	Metal cations	Qmax (mg g ⁻¹)	References
Monterey trees (<i>Pinus radiata</i>)	CHO acidifient	Pb ²⁺ Cd ²⁺	107.4 105.6	[39]
European Black Ecores <i>Pinus nigra</i>	HCl NaOH Fenton oxidation Chloroform Acetone Diethyl ether Ethanol Tetra ethylene glycol	Pb ²⁺ /Cd ²⁺	Pb ²⁺ /Cd ²⁺ 6.21/4.14 24.86/12.43 2486/11.39 0.16/9.32 13.46/8.28 19.68/11.39 12.43/7.25	[40]
Orange peel	Isopropanol Isopropanol + NaOH Citric acid	Pb ²⁺	70.44 107.7 70.44	[41]
Moringa leaves <i>Moringa oleifera</i>	NaOH	Pb ²⁺	186.48	[42]
Cellulosic fibre <i>Typha latifolia</i>	Untreated Treated H ₂ SO ₄	Pb ²⁺	32.64 44.65	This work

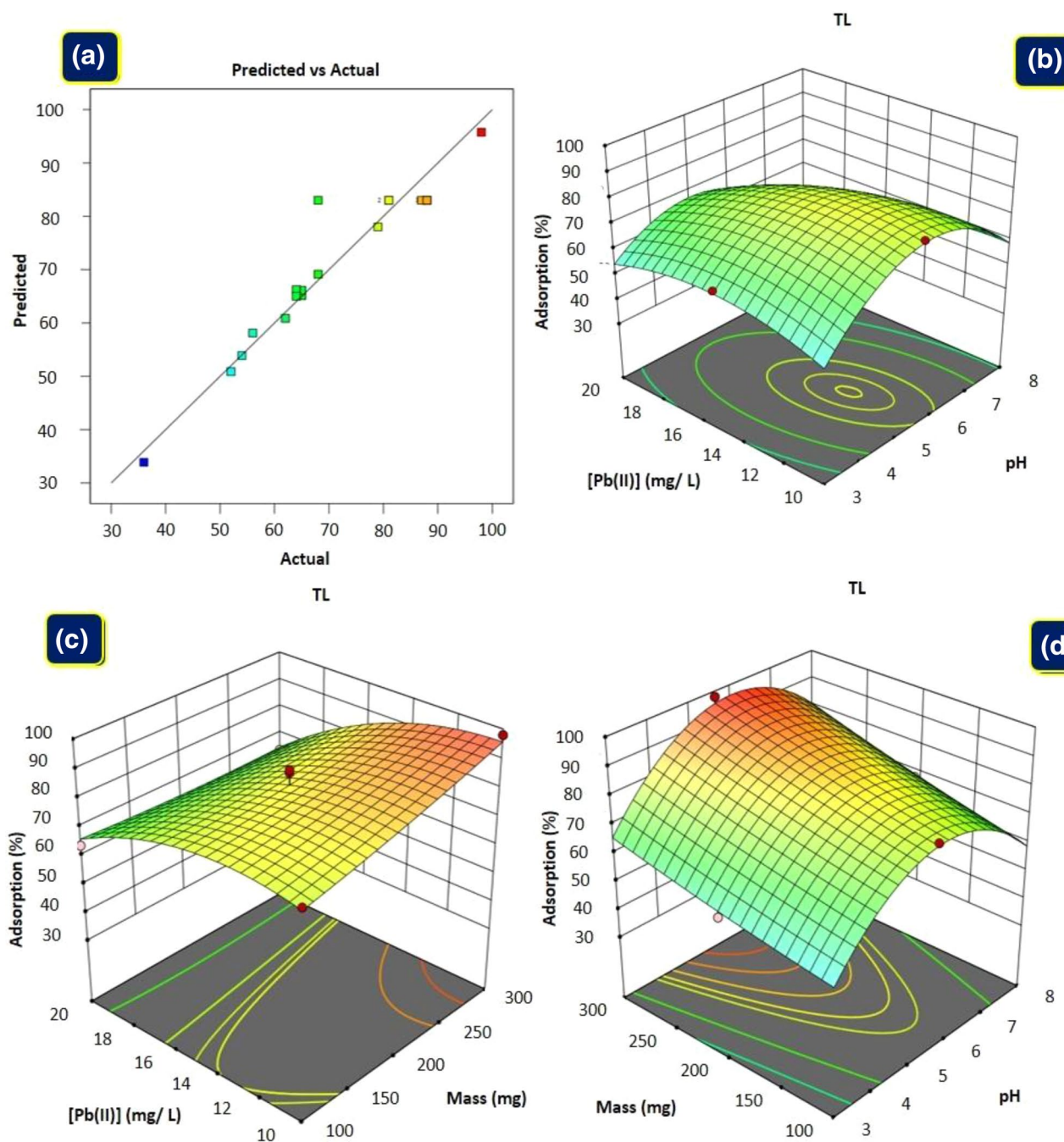


Fig. 17 **a** Effective versus expected responses, 3D response surface curves, **b** starting concentration of Pb (II) and solution pH (conditions: adsorbent mass of 0.1 g, 90 min contact time and 25 °C temperature), **c** starting concentration of Pb (II) and mass of biosorbent

(conditions: pH=5, 60 min contact time and 25 °C temperature), **d** mass of biosorbent and pH of solution (conditions: concentration of 10 ppm, 60 min contact time and 20 °C temperature) attained by employing BBD-RSM modeling for Pb (II) removal efficiency by *Tl*

many categories of alteration, although these data are far from complete; a study on *Citrus reticulata* biomass waste includes some chemical modifications. The fact that these doubled the q_{\max} values suggests that their effectiveness is just limited. The results obtained lead to a material with an improved retention capacity of 2.3%. Carbonisation of

plant material is just one of many physical processes that have been suggested. Examples include Coco149 and Ceiba pentandra fruit shells, as well as food, rice bran and many types of wood: The properties of the activated carbons produced also depend on the activation method (HCl, Na_2CO_3).

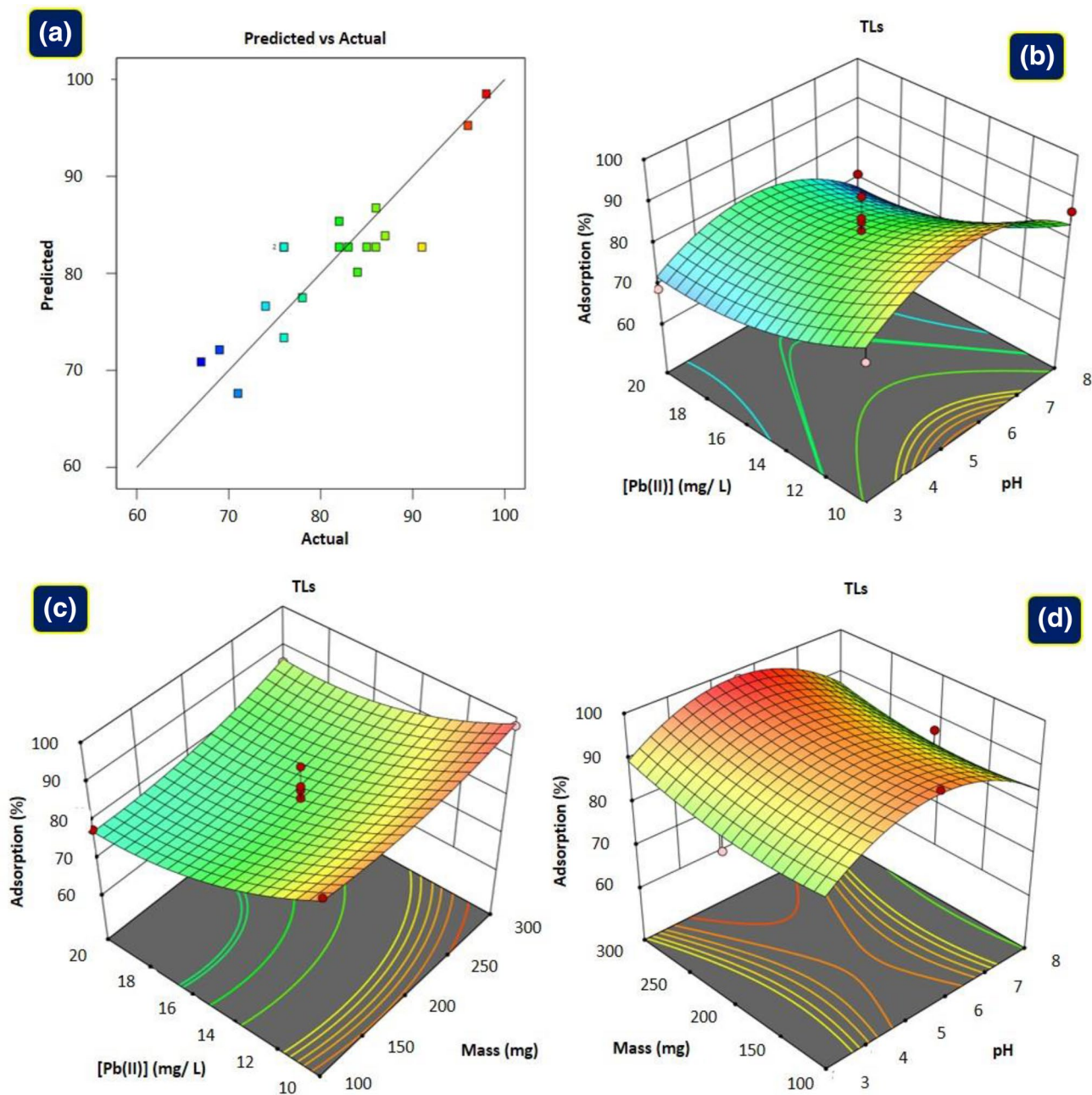


Fig. 18 **a** Real versus expected responses, 3D response surface curves, **b** starting Pb^{2+} concentration and solution pH (conditions: 0.1 g adsorbent mass, 40 min contact time, and 25 °C temperature), **c** starting Pb (II) concentration and *Tls* biosorbent mass (conditions:

pH=6, 40 min contact time, and 25 °C temperature), **d** *Tls* biosorbent mass and solution pH (conditions: Pb^{2+} concentration of 10 ppm, contact time of 40 min and temperature of 40 °C) resulting from use of BBD-RSM modeling for Pb (II) removal efficiency by *Tls*

3.10 Statistical Optimization of Pb (II) by the Biosorption Process

To maximize the effectiveness of lead extraction and to investigate the impacts of specific operating parameters interacting with one another, statistical optimization for lead biosorption on *Tl* and *Tls* was performed. The link between

the chosen variables (pH: A, mass: B, and initial Pb^{2+} concentration: C) and projected responses was represented by a quadratic polynomial model. Figures 17a and 18a show the results of the experiment and the anticipated reactions (a) The model created below was used to determine the projected Pb^{2+} biosorption efficiency:

Table 7 ANOVA data for designed model of Pb²⁺ biosorption onto *Tl* biosorbent

Source	Sum of squares	df	Mean Square	F value	p value
Model	4133.43	9	459.27	11.80	0.0005
A-pH	18.00	1	18.00	0.4625	0.0036
B-Mass	136.12	1	136.12	3.50	0.0943
C-[Pb(II)]	903.12	1	903.12	23.21	0.0010
AB	16.00	1	16.00	0.4111	0.0074
AC	196.00	1	196.00	5.04	0.0515
BC	90.25	1	90.25	2.32	0.1621
A ²	2242.87	1	2242.87	57.63	<0.0001
B ²	3.43	1	3.43	0.0881	0.0733
C ²	260.47	1	260.47	6.69	0.0294
Residual	350.25	9	38.92		
Lack of fit	26.25	3	8.75	0.1620	0.9181
Pure error	324.00	6	54.00		
Cor total	4483.68	18			
Model statistics	R ²	Adjusted R ²	Predicted R ²		Adequate precision
	0.9219	0.8438	0.8080		13.6718

Table 8 ANOVA data for designed model of Pb²⁺ biosorption onto *Tls*

Source	Sum of squares	df	Mean square	F value	p value
Model	1037.45	9	115.27	4.94	0.0026
A-pH	18.00	1	18.00	0.6156	0.0045
B-Mass	78.12	1	78.12	2.67	0.0013
C-[Pb (II)]	435.12	1	435.12	14.88	0.0039
AB	0.2500	1	0.2500	0.0085	0.9284
AC	2.25	1	2.25	0.0769	0.7877
BC	9.00	1	9.00	0.3078	0.5926
A ²	435.29	1	435.29	14.89	0.0039
B ²	25.65	1	25.65	0.8772	0.0037
C ²	86.45	1	86.45	2.96	0.1197
Residual	263.18	9	29.24		
Lack of Fit	87.75	3	29.25	1.00	0.4546
Pure Error	175.43	6	29.24		
Cor Total	1300.63	18			
Model statistics	R ²	Adjusted R ²	Predicted R ²		Adequate precision
	0.8977	0.9535	0.9631		7.8701

$$\begin{aligned}
 \text{Pb}^{2+}\% \text{Removal by TL} &= + 83.00 - 1.50 * A + 4.12 * B \\
 &- 10.63 * C + 2.00 * AB - 7.00 * AC \\
 &- 4.75 * BC - 22.37 * A^2 \\
 &+ 0.8750 * B^2 - 7.63 * C^2 \\
 \\
 \text{Pb}^{2+}\% \text{Removal by Tls} &= + 82.71 - 1.50 * A + 3.12 * B - 7.38 * C \\
 &- 0.2500 * AB - 0.7500 * AC \\
 &+ 1.50 * BC - 9.86 * A^2 \\
 &+ 2.39 * B^2 + 4.39 * C^2
 \end{aligned}$$

The ANOVA data is a useful tool for investigating the relevance of the model proposed above. Fisher's F-test results in Tables 7 and 8, which show that the created model was significant with just 0.01% noise, and low probability value (0.0005) [4]. If the p-values are less than 0.05, the term coefficients in the projected model are significant. The Pb ion removal process is significantly impacted by the *Tl* coefficients (A, C, AB, A², and C²) and *Tls* coefficients (A, B, C, A², and B²) in this research. The other *Tl* coefficients (B, AC, BC, and B²) as well as *Tls* (AB, AC, BC, and C²), on the other hand, were not. Furthermore, the R² and adjusted R² values were (0.921 and 0.843) for *Tl* and (0.897 and 0.9535)

for *Tls*, respectively, indicating that the model development demonstrated good lead ion biosorption behavior on *Tl* and *Tls*. Prediction. The appropriate precision values of 11.8 and 4.94 (> 4) *Tls*, respectively, were used to confirm the sufficiency and applicability of the model explaining the Pb^{2+} biosorption mechanism. The observed Pb^{2+} removal efficiency values are near to a straight line, which can be observed in the graph of actual against projected responses presented in Figs. 17a and 18a. This shows that the experimental results and the intended model agree. It is clear from the quadratic polynomial model's coefficient values that all of the chosen operational parameters had a significant impact on the removal efficiency of Pb ions.

The most important factor, with a value of 23.21 for *Tl* and 14.88 for *Tls*, was the starting Pb concentration (C). The negative sign demonstrated that the Pb ion concentration has an inverse correlation with the Pb^{2+} removal efficiency. The positive sign of their coefficients for the solution pH (A) and the increasing biosorbent mass (B) indicated that these parameters had a favorable impact on the biosorption of Pb^{2+} ions [43]. The created model demonstrated the presence of a potentially detrimental interaction between pH and Pb concentration ($\alpha_{23} = -4.75$ for *Tl*) ($\alpha_{23} = 1.50$ for *Tls*), weak interaction between Pb^{2+} concentration and biomass mass ($\alpha_{13} = -7.00$ for *Tl*) ($\alpha_{13} = -0.7500$ for *Tls*), and strong positive interaction between pH and biomass mass ($a_{12} = 2.00$ for *Tl*) ($a_{12} = -0.2500$ for *Tls*).

Furthermore, the effect of the interaction between Pb^{2+} ions on concentration and pH is shown in Figs. 17b and 18b. It is clear that as the pH value rises, the efficiency of removing lead rises as well. However, at pH = 7, lead begins to precipitate as $Pb(OH)_2$, resulting in an adverse effect on the efficiency of removing lead ions of Pb (II). Yet, the biosorption decreased as the initial Pb (II) content rose. For the initial Pb (II) concentration of 10 ppm at pH = 5, biosorption efficiencies of 77.6% and 96.8% were found for *Tl* and *Tls*, respectively. Figures 17c and 18c show the cumulative influence of biosorbent mass and starting Pb (II) concentration on the biosorption process (c). The adsorption performance of Pb (II) rises with increasing adsorbent mass, according to the 3D response surface curves. Whereas the removal effectiveness was negatively impacted by the initial Pb (II) concentration [42]. Consequently, a higher-quality 0.1 g biosorbent and a lower Pb^{2+} concentration was used to obtain the maximum Pb removal (77.6% *Tl*) (96.8% *Tls*) (10 ppm). A graphic illustration of the cumulative impact of biosorbent quality and pH on Pb removal effectiveness can be found in Figs. 17d and 18d. It is evident that pH and biosorbent quality have a beneficial impact on Pb (II) ion adsorption. Under alkaline conditions, higher amounts of biosorbent achieved the best response. Last but not least, under ideal conditions (pH = 5, biosorbent mass of 0.1 g, and

Pb^{2+} concentration of 10 ppm), the maximum % of Pb (II) elimination was attained.

4 Conclusion

The pH, adsorbent dosage, contact time, Pb (II) ion concentration, and temperature were found to be important influences on the Pb (II) ion adsorption on the *Typha latifolia* and activated *Typha latifolia* fibers of the reed plant filter. The outcomes are as follows: For both the untreated and treated resin of the reed filter, pH 5 was determined to be the best value for Pb (II) extraction. Adsorption rate went up as biosorbent dosage was increased, but it reduced as Pb (II) ion concentration was raised. Equilibrium took 60 and 40 min, respectively, for untreated and treated *Typha latifolia* fibers. The pseudo-second order model was followed during the adsorption. The Langmuir isotherm model, with a maximum adsorption capacity of 31.94 mg g^{-1} for untreated reeds and 46.0 mg g^{-1} for treated reeds, aptly represents the adsorption process. The separation factor (*Typha latifolia*) values ranged from 0 to $R_L < 1$, demonstrating the favorability of the adsorption procedure. The adsorption mechanism was demonstrated to be practicable, spontaneous, and exothermic using thermodynamic parameters such as G° , S , and H° . The findings of the current study demonstrated that the chemical pretreatment we developed can be employed as efficient adsorbents to extract Pb (II) ions from wastewater. Utilizing RSM statistical modeling, the Pb^{2+} adsorption rate on *Typha latifolia* (*Tl*) was optimized. The pH value of 6, 0.1 g *Typha latifolia* test, and 10 ppm Pb^{2+} ion concentration for 40 min at 25 °C resulted in the maximum removal effectiveness of (96.8%). According to the regeneration investigation, both *Typha latifolia* (*Tl*) and (*Tls*) have high reusability for removing Pb (II) ions from aqueous solutions. Overall, *Typha latifolia* have the potential to be a useful and affordable biosorbent for treating effluents that have been polluted with the Pb (II) contaminant.

Supplementary Information The online version contains supplementary material available at <https://doi.org/10.1007/s42250-023-00733-0>.

References

- Jin Y, Teng C, Yu S, Song T, Dong L, Liang J, Bai X, Liu X, Hu X, Qu J (2018) Batch and fixed-bed biosorption of Cd(II) from aqueous solution using immobilized *Pleurotus ostreatus* spent substrate. Chemosphere 191:799–808
- Ghaedi AM, Ghaedi M, Vafaei A, Irvani N, Keshavarz M, Rad M, Tyagi I, Agarwal S, Gupta VK (2015) Adsorption of copper (II) using modified activated carbon prepared from Pomegranate wood: optimization by bee algorithm and response surface

- methodology. *J Mol Liq* 206:195–206. <https://doi.org/10.1016/j.molliq.2015.02.029>
3. Dallel R, Kesraoui A, Seffen M (2018) Biosorption of cationic dye onto “*Phragmites australis*” fibers: characterization and mechanism. *J Environ Chem Eng* 6:7247–7256. <https://doi.org/10.1016/j.jece.2018.10.024>
 4. Regti A, Lakbaibi Z, Ben El Ayouchia H, El Haddad M, Laamari MR, El Himri M, Haounati R (2021) Hybrid methods combining computational and experimental measurements for the uptake of eriochrome black T dye utilising fish scales. *Int J Environ Anal Chem*. <https://doi.org/10.1080/03067319.2021.1929199>
 5. Haounati R, Ouachtak H, El Haouti R, Akhouairi S, Largo F, Akbal F, Benlhachemi A, Jada A, Addi AA (2021) Elaboration and properties of a new SDS/CTAB@Montmorillonite organoclay composite as a superb adsorbent for the removal of malachite green from aqueous solutions. *Sep Purif Technol* 255:117335. <https://doi.org/10.1016/j.seppur.2020.117335>
 6. Kang J-K, Lee S-C, Kim S-B (2018) Enhancement of selective Cu(II) sorption through preparation of surface-imprinted mesoporous silica SBA-15 under high molar concentration ratios of chloride and copper ions. *Microporous Mesoporous Mater* 272:193–201. <https://doi.org/10.1016/j.micromeso.2018.06.038>
 7. Gupta S, Sharma SK, Kumar A (2019) Biosorption of Ni(II) ions from aqueous solution using modified *Aloe barbadensis* Miller leaf powder. *Water Sci Eng* 12:27–36. <https://doi.org/10.1016/j.wse.2019.04.003>
 8. Ouachtak H, Akhouairi S, Haounati R, Addi AA, Jada A, Taha ML, Douch J (2020) 3,4-Dihydroxybenzoic acid removal from water by goethite modified natural sand column fixed-bed: experimental study and mathematical modeling. *Desalin Water Treat* 194:439–449. <https://doi.org/10.5004/dwt.2020.25562>
 9. Haounati R, El Guerdaoui A, Ouachtak H, El Haouti R, Boudouch A, Hafid N, Bakiz B, Santos DMF, Labd Taha M, Jada A, Ait Addi A (2021) Design of direct Z-scheme superb magnetic nanocomposite photocatalyst $\text{Fe}_3\text{O}_4/\text{Ag}_3\text{PO}_4$ @Sep for hazardous dye degradation. *Sep Purif Technol* 277:119399. <https://doi.org/10.1016/j.seppur.2021.119399>
 10. Vishan I, Saha B, Sivaprakasam S, Kalamdhad A (2019) Evaluation of Cd(II) biosorption in aqueous solution by using lyophilized biomass of novel bacterial strain *Bacillus badius* AK: biosorption kinetics, thermodynamics and mechanism. *Environ Technol Innov* 14:100323. <https://doi.org/10.1016/j.eti.2019.100323>
 11. Rangabhashiyam A, Lata S, Balasubramanian P (2018) Biosorption characteristics of methylene blue and malachite green from simulated wastewater onto *Carica papaya* wood biosorbent. *Surf Interfaces* 10:197–215. <https://doi.org/10.1016/j.surfin.2017.09.011>
 12. Kadiri L, Ouass A, Essaadaoui Y, Rifi EH, Lebki A (2018) *Coriandrum sativum* seeds as a green low-cost biosorbent for methylene blue dye removal from aqueous solution: spectroscopic, kinetic and thermodynamic studies. *Mediterr J Chem* 7:204–216. <https://doi.org/10.13171/mjc731810911-kadiri>
 13. Kankılıç GB, Metin AÜ, Tüzün İ (2016) *Phragmites australis*: an alternative biosorbent for basic dye removal. *Ecol Eng* 86:85–94. <https://doi.org/10.1016/j.ecoleng.2015.10.024>
 14. Tan B, Ching Y, Poh S, Abdullh L, Gan S (2015) A review of natural fiber reinforced poly(vinyl alcohol) based composites: application and opportunity. *Polymers* 7:2205–2222. <https://doi.org/10.3390/polym7111509>
 15. Kozlov VA, Nikiforova TE, Loginova VA, Koifman OI (2015) Mechanism of protodesorption—exchange of heavy metal cations for protons in a heterophase system of H_2O – H_2SO_4 – MSO_4 —cellulose sorbent. *J Hazard Mater* 299:725–732. <https://doi.org/10.1016/j.jhazmat.2015.08.004>
 16. El-Sheikh AH, Alshamaly HS (2020) Cadmium removal from organic acid-bearing soil-washing water by magnetic biosorption: effect of various factors and adsorption isothermal study. *J Environ Chem Eng* 8:104188. <https://doi.org/10.1016/j.jece.2020.104188>
 17. Zhang K, Khan A, Sun P, Zhang Y, Taraqqi-A-Kamal A, Zhang Y (2020) Simultaneous reduction of Cr(VI) and oxidation of organic pollutants by rice husk derived biochar and the interactive influences of coexisting Cr(VI). *Sci Total Environ* 706:135763. <https://doi.org/10.1016/j.scitotenv.2019.135763>
 18. Bediako JK, Wei W, Yun Y-S (2016) Conversion of waste textile cellulose fibers into heavy metal adsorbents. *J Ind Eng Chem* 43:61–68. <https://doi.org/10.1016/j.jiec.2016.07.048>
 19. Flauzino Neto WP, Silvério HA, Dantas NO, Pasquini D (2013) Extraction and characterization of cellulose nanocrystals from agro-industrial residue – soy hulls. *Ind Crops Prod* 42:480–488. <https://doi.org/10.1016/j.indcrop.2012.06.041>
 20. Maisyarah MA, Shiun LJ, Nasir AF, Haslenda H, Shin HW (2019) Characteristics of cellulose, hemicellulose and lignin of md2 pineapple biomass. *Chem Eng Trans* 72:79–84. <https://doi.org/10.3303/CET1972014>
 21. Bazargan-Lari R, Zafarani HR, Bahrololoom ME, Nemati A (2014) Removal of Cu(II) ions from aqueous solutions by low-cost natural hydroxyapatite/chitosan composite: equilibrium, kinetic and thermodynamic studies. *J Taiwan Inst Chem Eng* 45:1642–1648. <https://doi.org/10.1016/j.jtice.2013.11.009>
 22. Banerjee M, Basu RK, Das SK (2018) Cr(VI) adsorption by a green adsorbent walnut shell: adsorption studies, regeneration studies, scale-up design and economic feasibility. *Process Saf Environ Prot* 116:693–702. <https://doi.org/10.1016/j.psep.2018.03.037>
 23. Barquilha CER, Cossich ES, Tavares CRG, Silva EA (2019) Biosorption of nickel(II) and copper(II) ions by *Sargassum* sp. in nature and alginate extraction products. *Bioresour Technol Rep* 5:43–50. <https://doi.org/10.1016/j.biteb.2018.11.011>
 24. Albert Q, Leleyter L, Lemoine M, Heutte N, Rioult J-P, Sage L, Baraud F, Garon D (2018) Comparison of tolerance and biosorption of three trace metals (Cd, Cu, Pb) by the soil fungus *Absidia cylindrospora*. *Chemosphere* 196:386–392. <https://doi.org/10.1016/j.chemosphere.2017.12.156>
 25. Meitei MD, Prasad MNV (2014) Adsorption of Cu (II), Mn (II) and Zn (II) by *Spirodela polyrhiza* (L.) Schleiden: equilibrium, kinetic and thermodynamic studies. *Ecol Eng* 71:308–317. <https://doi.org/10.1016/j.ecoleng.2014.07.036>
 26. do Nascimento JM, de Oliveira JD, Rizzo ACL, Leite SGF (2019) Biosorption Cu (II) by the yeast *Saccharomyces cerevisiae*. *Biotechnol Rep* 21:00315. <https://doi.org/10.1016/j.btre.2019.e00315>
 27. Tabaraki R, Nateghi A (2014) Multimetal biosorption modeling of Zn²⁺, Cu²⁺ and Ni²⁺ by *Sargassum ilicifolium*. *Ecol Eng* 71:197–205. <https://doi.org/10.1016/j.ecoleng.2014.07.031>
 28. Shi Y, He J, Yang X, Zhou W, Wang J, Li X, Liu C (2019) Sorption of U(VI) onto natural soils and different mineral compositions: the batch method and spectroscopy analysis. *J Environ Radioact* 203:163–171. <https://doi.org/10.1016/j.jenvrad.2019.03.011>
 29. Yan J, Zhu Y, Qiu F, Zhao H, Yang D, Wang J, Wen W (2016) Kinetic, isotherm and thermodynamic studies for removal of methyl orange using a novel β -cyclodextrin functionalized graphene oxide-isophorone diisocyanate composites. *Chem Eng Res Des* 106:168–177. <https://doi.org/10.1016/j.cherd.2015.12.023>
 30. Bensalah J, Berradi M, Habsaoui A, Allaoui M, Essebaai H, El Khattabi O, Lebki A, Rifi E-H (2021) Kinetic and thermodynamic study of the adsorption of cationic dyes by the cationic

- artificial resin Amberlite®IRC50. Mater Today Proc 45:7468–7472. <https://doi.org/10.1016/j.matpr.2021.02.028>
31. El Alouani M, Alehyen S, El Achouri M, Taibi M (2018) Removal of cationic dye—methylene blue from aqueous solution by adsorption on fly ash based geopolymer. J Mater Environ Sci 9:32–46. <https://doi.org/10.26872/jmes.2018.9.1.5>
 32. Zheng L, Meng P (2016) Preparation, characterization of corn stalk xanthates and its feasibility for Cd (II) removal from aqueous solution. J Taiwan Inst Chem Eng 58:391–400. <https://doi.org/10.1016/j.jtice.2015.06.017>
 33. Basu M, Guha AK, Ray L (2017) Adsorption behavior of cadmium on husk of lentil. Process Saf Environ Prot 106:11–22. <https://doi.org/10.1016/j.psep.2016.11.025>
 34. Jabar JM, Adebayo MA, Owokotomo IA, Odusote YA, Yilmaz M (2022) Synthesis of high surface area mesoporous ZnCl₂-activated cocoa (*Theobroma cacao* L.) leaves biochar derived via pyrolysis for crystal violet dye removal. Heliyon 8:e10873. <https://doi.org/10.1016/j.heliyon.2022.e10873>
 35. Adebayo MA, Jabar JM, Amoko JS, Openiyi EO, Shodiya OO (2022) Coconut husk-raw clay-Fe composite: preparation, characteristics and mechanisms of Congo red adsorption. Sci Rep 12:14370. <https://doi.org/10.1038/s41598-022-18763-y>
 36. Kong Z, Li M, Chen J, Bao Y, Fan B, Francis F, Dai X (2016) Processing factors of triadimefon and triadimenol in barley brewing based on response surface methodology. Food Control 64:81–86. <https://doi.org/10.1016/j.foodcont.2015.12.021>
 37. Subha B, Song YC, Woo JH (2015) Optimization of biostimulant for bioremediation of contaminated coastal sediment by response surface methodology (RSM) and evaluation of microbial diversity by pyrosequencing. Mar Pollut Bull 98:235–246. <https://doi.org/10.1016/j.marpolbul.2015.06.042>
 38. Saelee K, Yingkamhaeng N, Nimchua T, Sukyai P (2016) An environmentally friendly xylanase-assisted pretreatment for cellulose nanofibrils isolation from sugarcane bagasse by high-pressure homogenization. Ind Crops Prod 82:149–160. <https://doi.org/10.1016/j.indcrop.2015.11.064>
 39. Argun ME, Dursun S, Karatas M (2009) Removal of Cd(II), Pb(II), Cu(II) and Ni(II) from water using modified pine bark. Desalination 249:519–527. <https://doi.org/10.1016/j.desal.2009.01.020>
 40. Norfahana A, Chuo Sing C, Siti Hamidah M-S, Umi AA, Khairul Faizal P, Kelly Yong TL (2020) Trends in adsorption mechanisms of fruit peel adsorbents to remove wastewater pollutants (Cu (II), Cd (II) and Pb (II)). J Water Environ Technol 18:290–313. <https://doi.org/10.2965/jwet.20-004>
 41. Xuan Z, Tang Y, Li X, Liu Y, Luo F (2006) Study on the equilibrium, kinetics and isotherm of biosorption of lead ions onto pretreated chemically modified orange peel. Biochem Eng J 31:160–164
 42. Reddy DHK, Harinath Y, Seshaiiah K, Reddy AVR (2010) Biosorption of Pb(II) from aqueous solutions using chemically modified *Moringa oleifera* tree leaves. Chem Eng J 162:626–634. <https://doi.org/10.1016/j.cej.2010.06.010>
 43. Largo F, Haounati R, Ouachtak H, Hafid N, Jada A, Ait Addi A (2023) Design of organically modified sepiolite and its use as adsorbent for hazardous Malachite Green dye removal from water. Water Air Soil Pollut 183:234. <https://doi.org/10.1007/s11270-023-06185-z>

Springer Nature or its licensor (e.g. a society or other partner) holds exclusive rights to this article under a publishing agreement with the author(s) or other rightsholder(s); author self-archiving of the accepted manuscript version of this article is solely governed by the terms of such publishing agreement and applicable law.